

1 **Influence of covariance of aerosol and meteorology on co-located precipitating and**
2 **non-precipitating clouds over Indo-Gangetic Plains**

3 Nabia Gulistan¹, Khan Alam^{1*}, Yangang Liu²

4 ¹Department of Physics, University of Peshawar, Peshawar, 25120, Pakistan

5 ²Environmental & Climate Science Department, Brookhaven National Laboratory, USA

6 *Correspondence: Khan Alam (khanalam@uop.edu.pk)

7 HIGHLIGHTS

- 8 • Strong aerosol-cloud relation under unstable meteorological conditions led to formation of
9 high-level thick clouds.
10 • In thick clouds the activation of cloud droplets is weakly dependent on aerosols.
11 • Optically thin clouds led to high precipitation rate.
12

13 ABSTRACT

14 Aerosol-cloud-precipitation-interaction (ACPI) plays a pivotal role in the global and regional
15 water cycle and the earth's energy budget; however, it remains highly uncertain due to the
16 underlying different physical mechanisms. Therefore, this study aims to systematically analyze the
17 effects of aerosols and meteorological factors on ACPI in the co-located precipitating (PCs) and
18 non-precipitating clouds (NPCs) clouds in winter and summer seasons by employing the long-term
19 (2001-2021) retrievals from Moderate Resolution Imaging Spectroradiometer (MODIS), Tropical
20 Rainfall Measuring Mission (TRMM), and National Center for Environmental Prediction/National
21 Center for Atmospheric Research (NCEP/NCAR) reanalysis-II datasets over the Indo-Gangetic
22 Plains (IGP). The results exhibit a decadal increase in aerosol optical depth (AOD) over Lahore
23 (5.2%), Delhi (9%), Kanpur (10.7%) and Gandhi College (22.7%) and decrease over Karachi (-
24 1.9%) and Jaipur (-0.5%). The most stable meteorology with high values of lower tropospheric
25 stability (LTS) is found in both seasons over Karachi. In summer season the occurrence frequency
26 of clouds is high (74%) over Gandhi College, 60% of which are PCs. Conversely, the least number
27 of PCs are found over Karachi. Similarly, in winter season, the frequency of cloud occurrence is
28 low over Karachi and high over Lahore and Gandhi College. The analysis of cloud top pressure
29 (CTP) and cloud optical thickness (COT) indicate high values of cloud fraction (CF) for thick and
30 high-level clouds over all study areas except Karachi. The micro-physical properties such as cloud
31 effective radius (CER) and cloud droplet number concentration (CDNC) bears high values (CER

32 $> \sim 15 \mu\text{m}$ and $\text{CDNC} > \sim 50 \text{ cm}^{-3}$) for both NPCs and PCs in summer. The AOD-CER correlation
33 is good (weak) for PCs (NPCs) in winter. Similarly, the sensitivity value of the first indirect effect
34 (FIE) is high (ranged from 0.2 ± 0.13 to 0.3 ± 0.01 in winter, and from 0.19 ± 0.03 to 0.32 ± 0.05
35 in summer) for PCs and low for NPCs. Sensitivity value for second indirect effect (SIE) is
36 relatively high (such as 0.6 ± 0.14 in winters and 0.4 ± 0.04 in summer) than FIE. Sensitivity values
37 of the aerosol-cloud interaction (ACI) are low (i.e., -0.06 ± 0.09) for PCs in summers. Furthermore,
38 the precipitation rate (PR) exhibits high values in summer season, and PR values are found high
39 in comparatively thin clouds with fewer CDNC ($< \sim 50 \text{ cm}^{-3}$) and intermediate for optically thick
40 clouds with higher CDNC ($> \sim 50 \text{ cm}^{-3}$).

41 **Keywords:** Aerosol-cloud-precipitation-interaction, Aerosol optical depth, cloud effective radius,
42 cloud droplet number concentration, lower tropospheric stability, relative humidity, first indirect
43 effect, second indirect effect, precipitation sensitivity.

44 1. Introduction

45 The aerosol-cloud-precipitation-interaction (ACPI) and aerosol-radiation-interaction (ARI)
46 significantly influence climates at the regional and global scales (Romero et al., 2021). Assessing
47 the direct and indirect effects of aerosols is crucial to understand and predict energy budget and
48 the water cycle. In the direct effect, the absorption and scattering of solar radiation by aerosols
49 lead to the warming of the atmosphere and cooling of the earth's surface (Zhou et al., 2020),
50 causing changes in the lower tropospheric stability (LTS) that further leads to modulation of
51 precipitating (PCs) and non-precipitation clouds (NPCs) (Andreae & Rosenfeld, 2008). In the
52 indirect effect, the water-soluble aerosols such as soil dust, sulfates, nitrates, and other organic
53 aerosols ejected naturally and anthropogenically serve as cloud condensation nuclei (CCN) and
54 ice nucleating particle (INP). Hence, aerosols affect the aerosol-cloud-interaction (ACI) by
55 influencing the growth of cloud droplet and cloud droplet number concentration (CDNC)
56 (Twomey et al., 1977; Albrecht, 1989; Jiang et al., 2002; Chen et al., 2011; Tao et al., 2012). The
57 increase of CDNC and decrease of cloud droplet effective radius (CER) inhibit the onset of
58 precipitation and increase the cloud lifetime (Albrecht, 1989). Conversely, the decrease in CDNC
59 and increase in CER increases the probability of precipitation rate (PR). Conversely, Stevens and
60 Feingold (2009) have shown that initially, more sea salt carried by high wind speed inhibit the

61 precipitation formation. However, the same sea spray tends to seed the coalescence by producing
62 larger CER that led to enhanced precipitation.

63 In the last few decades, most of the cultivable land of the Indo-Gangetic Plain (IGP) has been
64 replaced by urban developments. Due to the fastest growth of population, urbanization,
65 industrialization, and massive combustion of biomass and fossil fuels in residential homes and
66 factories, a decadal increase in aerosols is observed over IGP. The high aerosol loading may affect
67 the formation of tropospheric clouds and seasonal precipitation patterns (Kaskaoutis et al., 2011;
68 Singh et al., 2015; Thomas et al., 2021) and makes IGP suitable for the study of ACPI. Besides,
69 frequent variations in cloud fraction (CF), extreme precipitation and drought abrupt temperature
70 changes (e.g., heat waves), and irregular unseasonal rains may cause major and unavoidable
71 hazards at local and regional levels in the future.

72 In the last two decades, the scientific community has focused on quantification of ACI using both
73 observations (Feingold et al., 2003; Costantino et al., 2010; Zhao et al., 2018, 2020; Anwar et al.,
74 2022) and modeling techniques (Chen et al., 2016, 2018; Wang et al. 2020; Zhou et al., 2020;
75 Sharma et al., 2023). Although, a similar recent study (Anwar et al., 2022) attempted to understand
76 the sensitivities of ACI and the first indirect effect of different subsets of AOD to the different
77 conditions of RH and wind directions and found decrease (increase) in CER with aerosol loading
78 Twomey effect (anti-Twomey effect) over the monsoon (weak and moderately intensive monsoon)
79 regions. However, the above study excluded the other significant meteorological parameters such
80 as LTS, PR, and T_{850} and was also limited to the monsoon regions of Pakistan only. Further, in the
81 context of warm rain processes, it is generally understood that the high concentration of aerosols
82 capable of serving as CCN leads to enhanced CDNC known as the first indirect effect (FIE) or
83 Twomey effect (Twomey et al., 1977). It is also widely acknowledged that CDNC plays a pivotal
84 role in cloud microphysics and significantly influences the onset of precipitation and retention of
85 water in clouds called the second indirect effect (SIE) (Gryspeerd et al., 2016; Naud et al., 2017).
86 Whilst, in the above study, the analysis of CDNC is also not addressed. Therefore, the present
87 study aims to deepen the previous study (Anwar et al., 2022), by a long-term and detailed analysis
88 of the ACPI including aerosol-indirect effects for low-level clouds extended over the whole IGP
89 for understanding different mechanisms (condensation, droplet growth and precipitation rate) of
90 cloud and precipitation formation.

91 This study is focused on estimating the variations in sensitivities of aerosol-cloud relationship to
92 the variations in aerosol loading at specified meteorological conditions for low-level PCs and
93 NPCs in the summer and winter seasons over the IGP. This study is unique in using a large number
94 of samples, classification of liquid clouds in PCs and NPCs, further classification of clouds in low,
95 mid, and high-level clouds through joint COT-CTP histograms, quantification of the sensitivities
96 of FIE, SIE, total indirect effect (TIE), and ACI to CDNC. The significant meteorological
97 parameters considered include temperature at 850 hPa, LTS, relative humidity (RH%) at 850 hPa,
98 vertical velocity (Ω), and PR. Furthermore, by utilizing the Moderate Resolution Imaging
99 Spectroradiometer (MODIS) and Tropical Rainfall Measuring Mission (TRMM) data, the
100 correlation of cloud microphysical properties (CER and CDNC) and AOD at specified values of
101 LTS and cloud liquid water path (CLWP) is examined, and precipitation sensitivity at constant
102 macro-physical condition is estimated.

103 2. Study area and methodology

104 2.1. Study area

105 The selected study area (Fig. 1) comprises the upper, middle, and eastern portions of the IGP. The
106 upper part consists of the densely populated and developed regions of the eastern part of Pakistan
107 i.e., Karachi (24.87°N, 67.03°E) and Lahore (31.54°N, 74.32°E) whereas the middle part comprises
108 the northern part of India i.e., Delhi (28.59°N, 77.22°E), Kanpur (26.51°N, 80.23°E), Jaipur
109 (26.91°N, 75.81°E), Gandhi College (25.87°N, 84.13°E), Kolkata (22.57°N, 88.36°E), Dhaka
110 (23.80°N, 90.41°E) and Patna (25.59°N, 85.13°E). The data analysis for the eastern part of IGP
111 (Kolkata, Dhaka and Patna) is documented as supplementary materials.

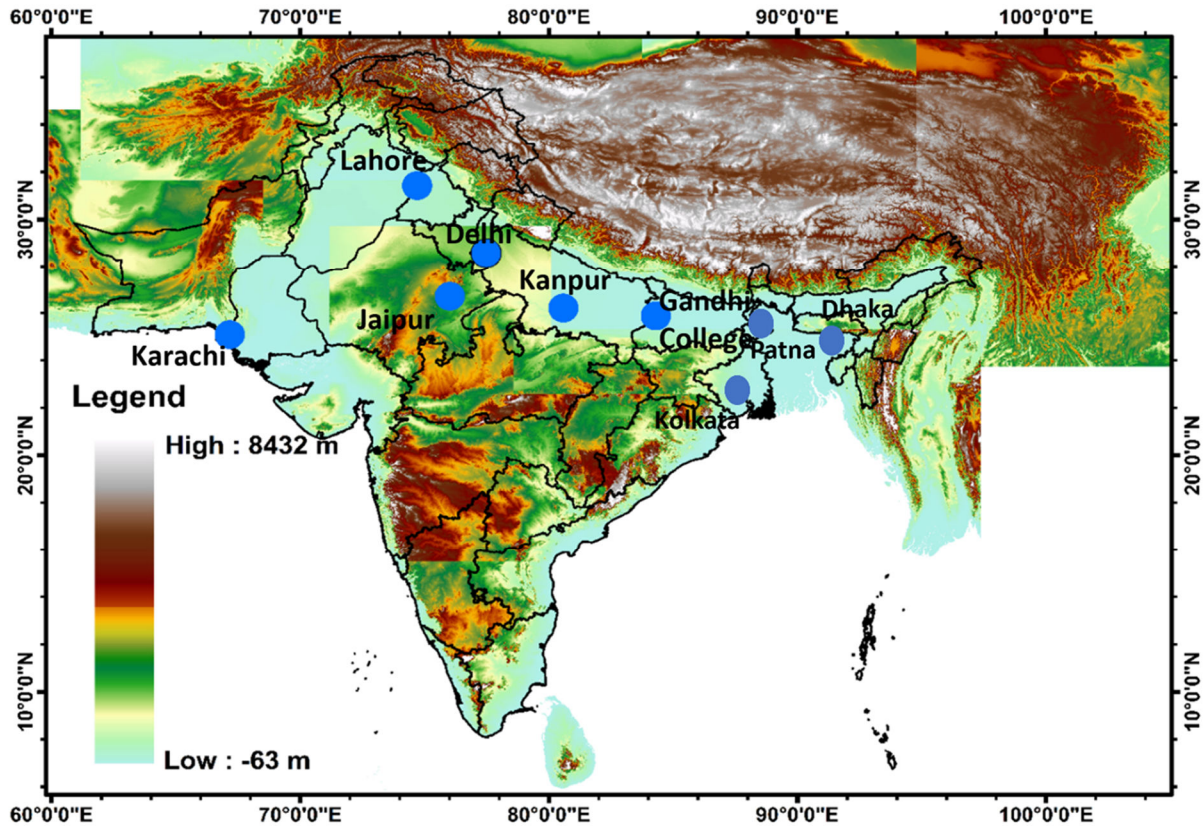


Figure 1. Topography of the study area.

2.2. Methodology

2.2.1. MODIS, NCEP/NCAR reanalysis-II and TRMM data

Moderate Resolution Imaging Spectroradiometer (MODIS) is a major constituent of NASA's Earth Observing System (EOS). MODIS is orbiting with two onboard satellites, Terra and Aqua, launched in 1999 and 2002 respectively, with a range of 2330 km spanning the entire globe in a day. It provides data and information with a spatial resolution of 1° to study atmospheric processes and physical structure (Kedia et al., 2014; Srivastava et al., 2015). This study uses the daily mean of combined dark target and deep blue AOD at $0.55 \mu\text{m}$, cloud top pressure (CTP), cloud top temperature (CTT), CF, CER, and COT for liquid clouds from level 3 aerosol-cloud data product MOD08-TERRA. Data with $\text{AOD} > 1.5$ are excluded to avoid potential misidentification of aerosols as clouds. The following adiabatic approximation (Brenquier et al., 2000; Wood, 2006; Kubar et al., 2009; Michibata et al., 2014) is used to calculate CDNC (cm^{-3}):

126
$$CDNC = \left(\frac{B}{CER} \right)^3 * \sqrt{(2 * CLWP * \gamma_{eff})}$$

127 (1)

128 Where $B = \sqrt[3]{\left(\frac{3}{4}\pi\rho_{water}\right)} = 0.0620$, ρ_{water} is the liquid water density, γ_{eff} is the adiabatic
 129 gradient of liquid water content in the moist air column (Wood, 2006). Value of γ_{eff} range from 1
 130 to 2.5×10^{-3} at a temperature of 32 K to 104 K (Brenguier, 1991; Zhu et al., 2018; Zhou et al.,
 131 2020). The CLWP is estimated by use of

132
$$CLWP = \frac{5\rho_w(CER)(COT)_w}{9},$$

133 (2)

134 Where, ρ_w is the water density at room temperature (Koike et al., 2016).

135 National Center for Environmental Prediction/National Center for Atmospheric Research
 136 (NCEP/NCAR) reanalysis datasets provide global reanalysis data sets that combine satellite
 137 observations with the simulation of models through data assimilation (Purdy et al., 2016). Daily
 138 data for meteorological parameters including temperature, RH%, and Ω at 850 hPa are retrieved
 139 at a spatial resolution of T62 Gaussian grid ($1.915^\circ \times 1.875^\circ$) from NCEP reanalysis-II datasets,
 140 and used to calculate lower tropospheric stability (LTS) defined as (Li et al., 2017):

141
$$LTS = \theta_{700} - \theta_{1000}$$

142 (3)

143 where θ is the potential temperature and the subscripts denote the pressure levels of 700
 144 hPa and 1000 hPa.

145 The Tropical Rainfall Measuring Mission (TRMM) is the first Joint satellite mission between
 146 NASA America and National Space Development Agency (NASDA) Japan, utilizing the visible
 147 infrared and microwaves to measure the rain precipitation over tropical and subtropical regions.
 148 The main TRMM instruments that are used to measure rain precipitation are **precipitation radar**
 149 **(PR)** and **TRMM Microwave Imager (TMI)**. Where PR is operating at a frequency of 13.8 GHz
 150 and TMI is a passive microwave radiometer consisting of nine channels. A calibrated data set
 151 TRMM-2B31 of TRMM Combined Instrument (TCI) for TRMM Multi-Satellite Precipitation
 152 Analysis (TMPA) is formed from an algorithm that uses TMI and PR. The product TMPA 3B42

153 gives the rain precipitation averages on a daily and sub-daily basis. In the current study, the data
 154 product TMPA or TRMM 3B42 is used for the retrieval of PR on daily basis. The spatial resolution
 155 of TRMM 3B42 is $0.25^\circ \times 0.25^\circ$ and is available from the year 1998 to till date.

156 2.2.2. Methodology

157 The present study is designed to analyze and quantify the ACPI for PCs and NPCs in winter and
 158 summer under a variety of meteorological conditions. The daily mean data of each parameter for
 159 warm clouds are retrieved from the respective satellites and NCEP/NCAR reanalysis-II for each
 160 study site. Subsequently, in this analysis, the VLOOKUP function is utilized for linear
 161 interpolation/alignment of the data. This function is available as a built-in feature in Microsoft
 162 Excel. The data are then segregated into two subsets for the summer and winter seasons. Based on
 163 precipitation data from TRMM, the subsets are further divided into precipitating and non-
 164 precipitating clouds.

165 The sensitivities of cloud parameters to CDNC are analyzed through the following formulation
 166 considered from previous studies (Zhou et al., 2020):

$$167 \frac{dln(COT)}{dln(CDNC)} = -\frac{dln(CER)}{dln(CDNC)} + \frac{dln(CLWP)}{dln(CDNC)} \quad (4)$$

168 In this study, the term on the left side of equation (3) is defined as total indirect aerosol effect
 169 (TIE), and the first and second terms on the right side of the equation are defined as the first indirect
 170 aerosol effect (FIE), and second indirect effect (SIE), respectively. Similarly, the sensitivity
 171 of CDNC to AOD is evaluated by employing the index of ACI:

$$172 ACI_{CDNC} = \frac{dln(CDNC)}{dln(AOD)} \quad (5)$$

173 The sensitivity of PR to CDNC is calculated from the following equation (Jung et al., 2012) :

$$174 S_0 = \left(-\frac{\partial ln(PR)}{\partial ln(CDNC)} \right)_{COT} \quad (6)$$

175 3. Results and Discussion

176 3.1. Regional and seasonal distribution of AOD

177 AOD is a commonly used proxy for aerosol concentration in the atmosphere and is analyzed here
178 (Fig. 2-3).

179 IGP characteristically exhibits a diverse and massive pool of aerosols due to its unique topography.
180 The western part of IGP is a coastal location and inlet for the westerly winds. Therefore, dry
181 regions and Arabian sea in the west contribute dust, sea salt and water vapors to the region. The
182 Himalayas in the north act as barriers to the winds, leading to the trapping of aerosols over the
183 central part of IGP. Therefore, this region exhibits a high concentration of anthropogenic aerosols.
184 Bay of Bengal in the east allows southeasterly winds to enter passing across Dhaka, Kolkata, Patna
185 to Delhi and Lahore (Hassan et al., 2002; Anwar et al., 2022). The westerly and easterly winds
186 traverse forested hilly terrain, rivers and lakes elevating humidity level and initiate the cloud
187 formation by activation of the newly originated small aerosol particles as CCNs and cloud
188 formation affecting the local microclimate.

189 Fig. 2 shows a decadal variation in time average maps for combined dark target and deep blue
190 AOD retrieved at $0.55 \mu\text{m}$ over the entire study area for the years (2001-2010) and (2011-2021).
191 Also, Table 1 illustrates the percentage change in decadal averaged values of AOD. The results
192 indicate that AOD exhibits a decrease over Karachi (-1.9%) and Jaipur (-0.5%). Whilst an increase
193 in AOD is observed over Lahore (5.2%), Delhi (9%), Kanpur (10.7%) and Gandhi College
194 (22.7%). Similarly, Table 1S shows the decadal change in AOD over Kolkata (18%), Dhaka
195 (22.6%) and Patna (23.3%). Similar to Gandhi College, an increase is observed over all the three
196 areas. Reason for the increase of aerosols include multiple sources of aerosols, human behavior,
197 socio-economic development at local and regional level, and unique topography for persistence
198 and retaining of aerosols.

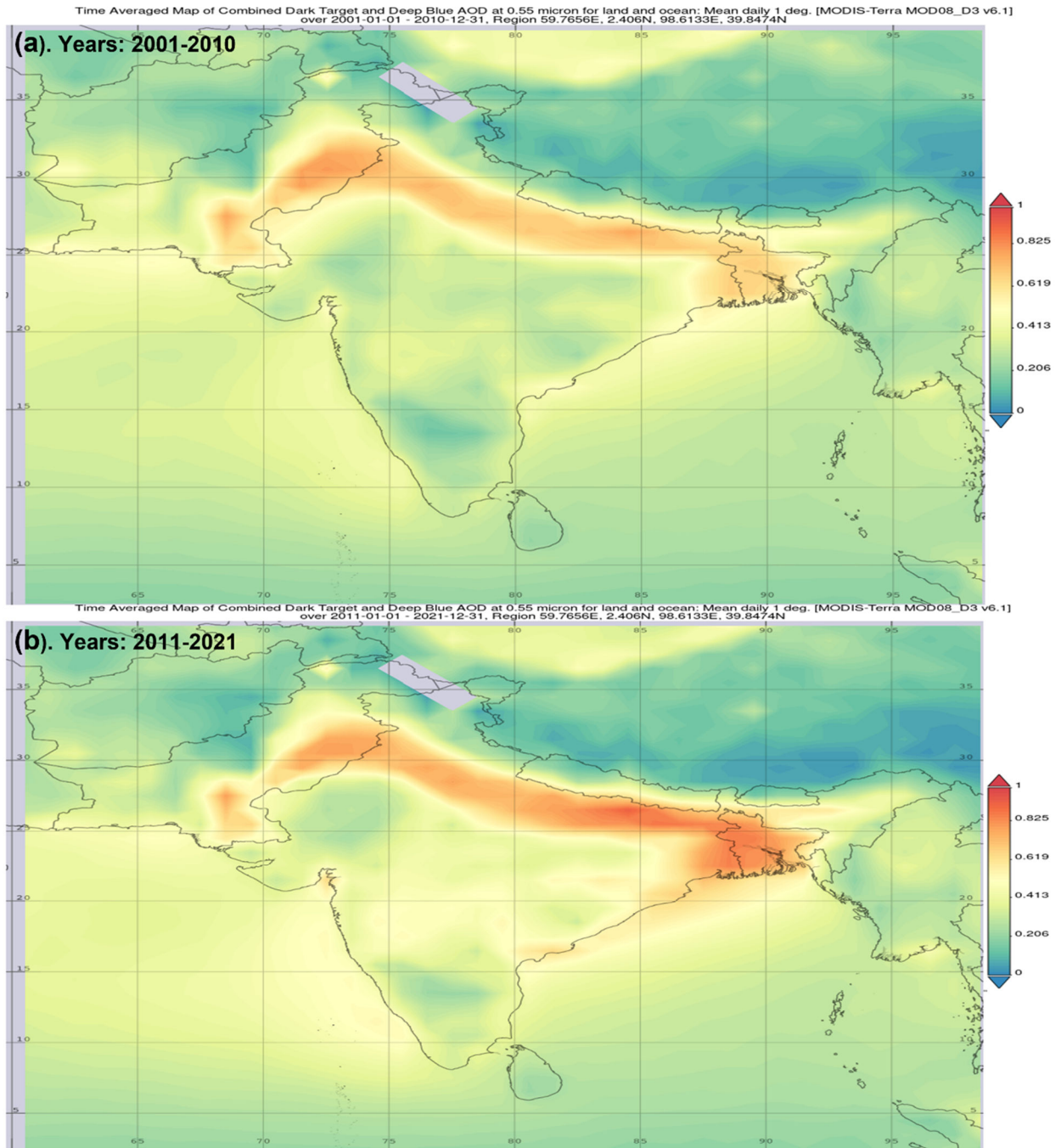
199 Fig.3(a-b) shows the probability density function (PDF) for AOD, illustrating different
200 distributions in summer and winter season. Fig.3a shows that the distribution of AOD over Delhi,
201 Kanpur, and Gandhi College is similar. However, a shift in peak value of PDF towards high values
202 of AOD over Lahore and low values over Jaipur illustrate comparatively high and low aerosol
203 concentration in summer season over Lahore and Jaipur respectively. Likewise, Fig. 1S shows the

204 seasonal PDF values of AOD over Kolkata, Dhaka and Patna. The results indicate similar seasonal
205 distribution functions over all the three areas of eastern IGP. In both seasons PDF peaks for high
206 values of AOD are observed over Patna showing high concentration of aerosols as compared to
207 Kolkata and Dhaka.

208 The loading of high concentration of aerosols is owing to the high-density of population,
209 industrialization, and human activities. The major sources of aerosols in all months of the year
210 include vehicular emission originated from old transport facilities, emission of smoke and soot
211 during consumption of biomass for cooking, heavy industrial emission, and aerosols produced in
212 seasonal harvesting and crop-residue burning. All these sources produce organic aerosols which are
213 characterized as hydrophilic particles and have the potential to act as CCN. Likewise, the soil dust
214 particles also act as good CCN due to their hygroscopic nature (Sun & Ariya, 2006). Moreover,
215 the meteorological conditions also play a substantial role to enhance AOD values such as the
216 uplifting of loose soil dust and swelling of aerosols due to holding the water vapors (wv) for long
217 time (Masmoudi et al., 2003; Alam et al., 2010; Alam et al., 2011;). Also, the lower but flat PDF
218 curve demonstrates low values of AOD over Karachi. Ali et al., 2020 associated the low AOD
219 values over Karachi to the westerly and southwesterly winds currents at tropospheric level.
220 However, the decreasing trend in AOD over the coastal city may also be attributed to the variations
221 in other meteorological parameters like T and RH.

222 As compared to summer season, the pattern of PDF in winter is significantly different as shown in
223 Fig. 3b. The low value of PDF (0.5) for the high value of AOD (0.9) over Karachi illustrates a
224 comparatively pristine atmosphere. Similarly, the PDF peaks for Lahore, Delhi and Jaipur (0.7, 0.7
225 and 0.8) indicate comparatively high AOD over Delhi. Likewise, the distribution over Kanpur and
226 Gandhi College is similar illustrating similar values of AOD (1.1 and 1.2 respectively). These high
227 values of AOD are attributed to the high emission of anthropogenic aerosols at local and regional
228 level over the central part of IGP (Delhi, Jaipur, Kanpur and Gandhi College).

229 Few authors attributed the reduced values of AOD in winter season to the wet scavenging and
230 suppressed emission of aerosols from earth surface (Alam et al., 2010; Zeb et al., 2019). However,
231 in our case, the low (high) values in winter (summer) are associated to dispersion of fine (course)
232 mode particles due to the variations in meteorological conditions.



233

234

Figure 2. Decadal increase (year: 2001-2010 and 2011-2021) in AOD over study sites.

235

236

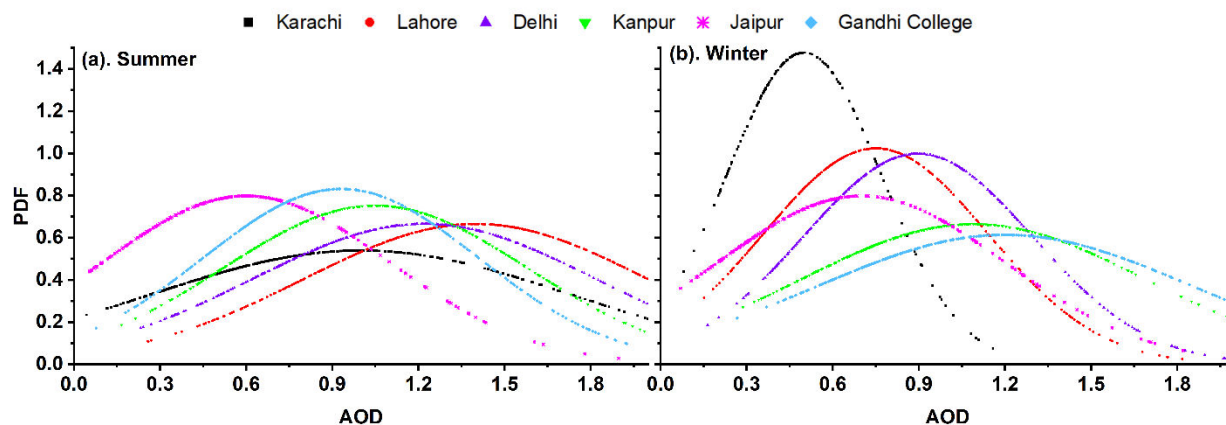
237

238

239 **Table 1.** Decadal percentage variations in average values of AOD over all study areas

	Karachi	Lahore	Delhi	Kanpur	Jaipur	Gandhi College
Total number of counts	5902	6171	5823	5201	5907	5125
Decadal change in AOD	-1.9%	5.2%	9%	10.7%	-0.5%	22.7%

240



241

242 **Figure 3.** Probability density function (PDF) of AOD over study sites is shown (a) and (b) for summer and winter
243 seasons respectively.

244 3.2. Climatology of meteorological parameters

245 Generally, LTS has relationships to factors such as temperature, humidity, wind patterns, and
246 atmospheric pressure over extended periods. It is also widely acknowledged that atmospheric
247 stability, temperature, RH and wind speed and direction play a significant role in cloud formation
248 (Yang et al., 2015; Tao et al., 2012). Therefore, the influence of long-term variations in the said
249 meteorological parameters are considered in the current study. The variations in meteorological
250 parameters have an unavoidable impact on ACPI. The parameters considered in this study include
251 the temperature, LTS to determine the lower atmospheric stability and instability that influence the
252 process of cloud and precipitation formation through its significant implications on evaporation
253 and convection of the air parcel, the RH% to estimate the level of wv and the Ω to assess the
254 suitable atmospheric dynamics. Fig.4 shows the variations in LTS values for NPCs and PCs in
255 winter and summer season. In winter season, the LTS values are high for NPCs and comparatively
256 lower for PCs over entire study areas. In summer season, the scenario is reversed with high values
257 for PCs but low values for NPCs, suggesting stable tropospheric layer on rainy days. This

258 stabilization may be attributed to the cold pools generated by the evaporation of falling rain
259 droplets (Wu et al., 2017). The lower LTS values for NPCs in summer season suggest the
260 likelihood of stronger instability that causes high potential of vertical motion and development of
261 thunderstorm. However, Karachi exhibits a distinct pattern of LTS with the highest values in each
262 case, which indicates the existence of the most stable tropospheric layer in Karachi due likely to
263 moist and cold sea breeze due to the city's coastal location.

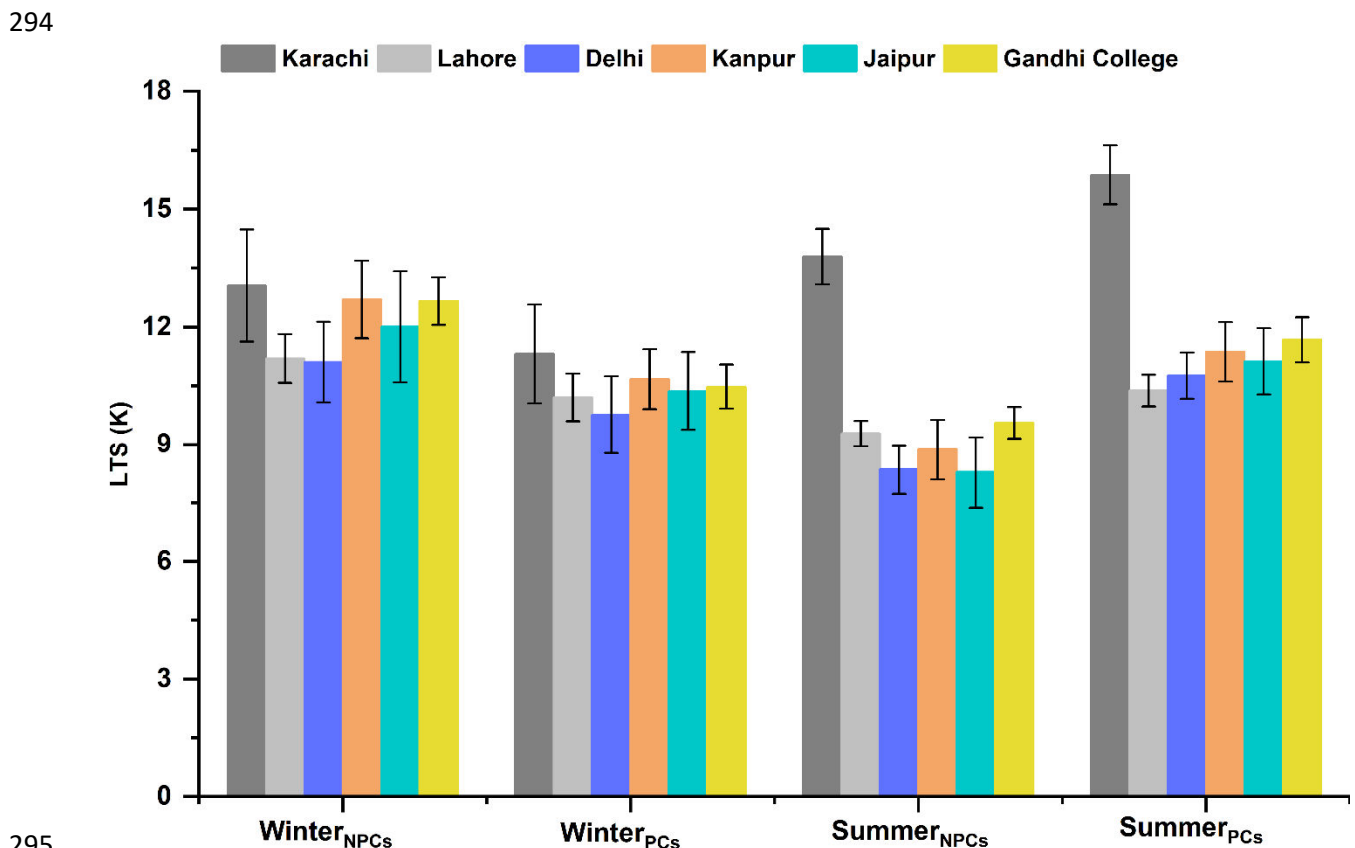
264 **The median values computed for the remaining meteorological parameters considered in this study**
265 **are listed in Table 2.** The high values in each case are indicated in bold and low values are italicized.
266 The results show that in winter season the temperature at 850 hPa (T_{850}) is relatively high for NPCs
267 ranging from **281 K** to **285.6 K**. The increase in RH% for PCs **during winter** ranged from **(59.5)%**
268 **to (71.5)%**. Also, the $\Omega > 0$ for NPCs and < 0 for PCs in winter season.

269 In summer season, it is observed that T_{850} is comparatively higher than that for the winter clouds
270 and ranged from **298.3 to 300.2 K** and **296.5 to 298.3 K** for NPCs and PCs respectively. The high
271 values of T_{850} are due to intense solar fluxes in summer season that keep the temperature of the
272 earth's surface and adjacent atmospheric layer higher. Also, the increase in RH% **during summer**
273 ranged between **33.5-51.7 % for NPCs**. The reason for the high values of wv and RH% is mainly
274 the suitable thermodynamical conditions **such as evaporation and convection due to the high**
275 **temperature of earth surface and air** (Sherwood et al., 2010). The results show high values of RH%
276 **70.1% (85%)** in winter (summer) season for PCs over Gandhi College. Conversely, notable
277 **fluctuations in RH% are observed over the coastal city, Karachi, with values of 71.5% (65.9%) in**
278 **winter (summer).** Similarly, Fig. 2S and Table 2S show the LTS conditions for PCs and NPCs. The
279 **high LTS values indicate more stable condition over Dhaka.** Similarly, Table 2S shows the seasonal
280 **average values for other meteorological parameters.** **The results indicate high values of T_{850} , RH%**
281 **and Ω 295.5 (297.5) K, 88.8 (83.5)% and -0.19 (-0.17) m/s respectively for PCs (NPCs) for over**
282 **Patna in summer.**

283 Besides, during the last two decades, the wv and fog over the Arabian Sea were increased (Verma
284 et al., 2022). Therefore, the high values of wv and RH% in summer months is due to the high-
285 speed zonal winds that blew in the summer season and transport water vapors and sea salt from
286 the surface of the Arabian Sea and hydrophilic aerosols such as soil dust from deserts of Iran,
287 Pakistan, and India to IGP. **Moreover, during the winter season, the elevated humidity levels are**

288 noticeable over IGP, particularly in the vicinity of Gandhi College. This increased humidity is a
 289 result of evapotranspiration driven by agricultural practices, irrigation, the presence of rivers and
 290 lakes, and the introduction of moist, cold air from western winds (Nair et al., 2020). Where $\Omega < 0$
 291 for PCs over all study areas except Karachi.

292 The distinct variations in meteorological parameters reveal the occurrence of clouds with diverse
 293 properties. The detailed analysis of such clouds is given in the next subsections.



295
 296 **Figure 4.** Variations in lower tropospheric stability (LTS) over all study sites for PCs and NPCs in winter and summer
 297 seasons, the error bars show the standard deviation (SD) values.

298 **Table 2.** Meteorological parameters for PCs(NPCs) in summer and winter seasons. Maximum values are for both types of clouds shown in bold
 299 and minimum values are indicated as italic.

	Winter Season			Summer Season		
	T ₈₅₀ (K)	RH%	Ω (m/s)	T ₈₅₀ (K)	RH%	Ω (m/s)
Karachi	284.6 (285.8)	71.5 (38)	-0.038 (<i>0.030</i>)	295.9 (298.8)	65.9 (45.9)	<i>0.005 (-0.003)</i>
Lahore	280.5 (<i>281.2</i>)	59.5 (35.5)	-0.02 (0.065)	298.3 (300.2)	65 (33.5)	-0.028 (<i>0.025</i>)
Delhi	284.2 (283.1)	60.2 (33.8)	-0.1 (0.04)	296.5 (299.4)	64.2 (42)	-0.05 (<i>-0.001</i>)
Kanpur	283.8 (284.1)	65.7 (36)	-0.1 (0.048)	296.5 (298.4)	73.7 (43.6)	-0.13 (<i>-0.08</i>)
Jaipur	283.9 (284.1)	66 (40.5)	-0.065 (0.049)	296.8 (298.7)	64 (51.7)	-0.04 (<i>-0.029</i>)
Gandhi College	283.2 (284.1)	70.1 (45.7)	-0.1 (0.05)	296.9 (298.3)	85 (42.5)	-0.16 (-0.11)

300

301

302

303

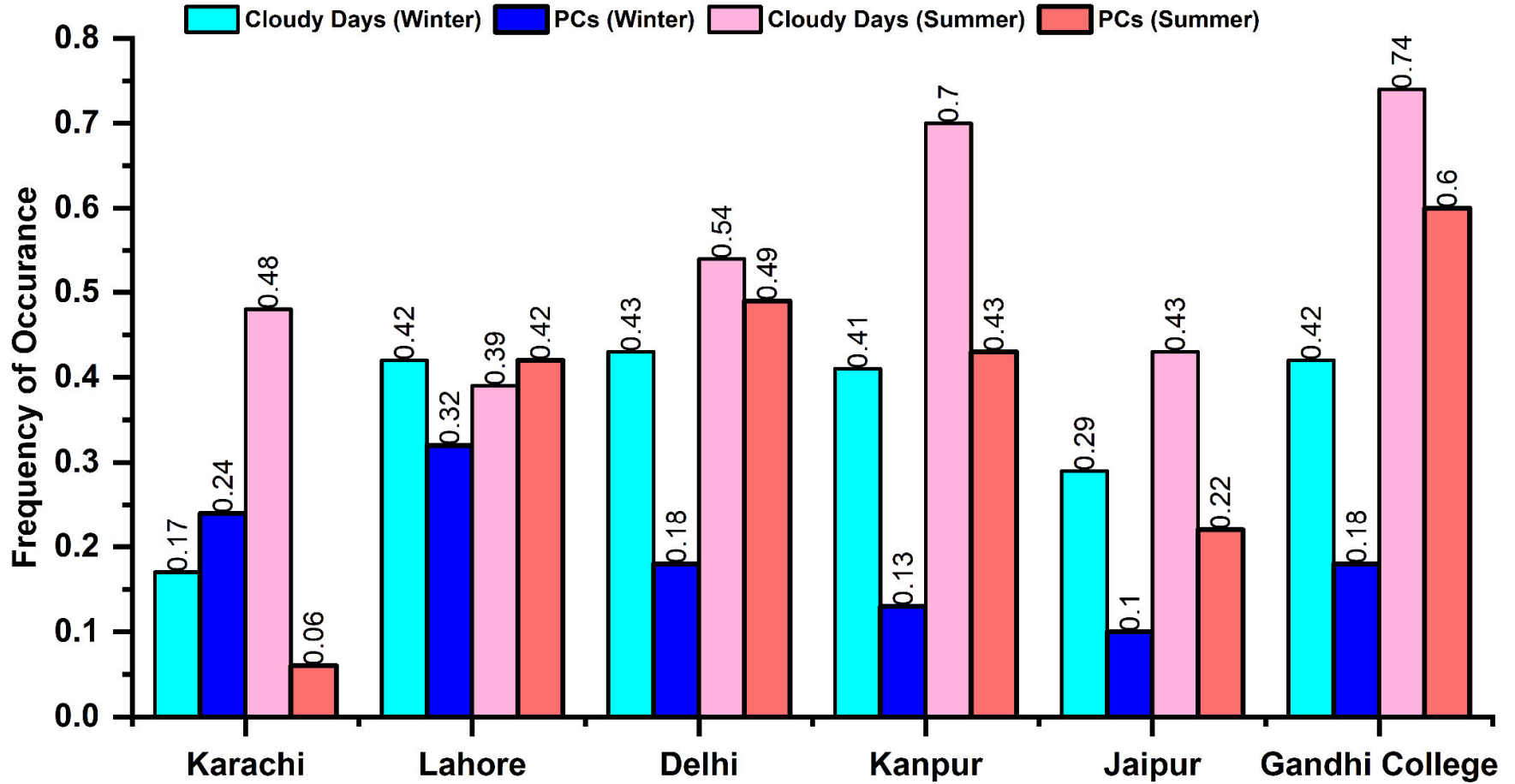
304

3.3. Regional and seasonal distribution of clouds and precipitations

3.3.1. Regional and seasonal differences in clouds occurrence and its microphysical structure

Fig.5 shows the frequency of occurrence of precipitable clouds and total number of cloudy days. Chen et al. (2018) suggested the COT to be the effective measure for assessing the clouds and potential for precipitation. In our case, to avoid any overestimation, the COT data are aligned with PR data on corresponding dates and then filtered to include $COT \sim > 5$ for PCs. The results show that in the winter season the frequency of clouds is low over Karachi and high over Lahore and Gandhi College. The results suggest the high number of PCs only over Lahore. In summer season, the high number i.e., 74 % of the total data counts over Gandhi College are identified as cloudy days, 60 % of which are PCs. Similarly, most of the clouds over Lahore, Delhi and Jaipur are PCs. Conversely, the least number of PCs (6 %) are found over Karachi. Likewise, Fig. 3S shows the total number of cloudy days and the number of days on which PCs occurred. The high occurrence of clouds is observed over Kolkata 83% (60%) and Dhaka 91% (69%) in summer (winter) season. The high occurrence of PCs in summer is due likely to the significant impact of elevated aerosols with the southwesterly winds on the summer monsoons and occurrence of PCs. Therefore, Kolkata and Dhaka are of critical importance from perspective of aerosol loading and ACI (Dahal et al., 2022).

323



325

326

Figure 5. Frequency of occurrence of total cloudy days (including PCs and NPCs) and only PCs is shown for both winter and summer seasons.

327 Table 3 shows the criteria adopted from previous papers (Rossow & Schiffer, 1999; Wyant et
328 al., 2006; Sharma et al., 2023) for further classification of NPCs and PCs into different type of
329 clouds. The aim of identifying the cloud types is to assess the cloud regimes and their vertical
330 structure for the better understanding of ACPI. In accordance with table 3, Fig. 6 shows joint
331 histograms of COT-CTP displaying the median values of CF for nine different types of clouds.
332 For a quick visual comparison, the cloud types are ordered from low to high level clouds. Also,
333 for each histogram, the bins of COT and CTP are located on x- and y-axis respectively. While
334 the CF of each bin is represented with the colored bar with its value mentioned in the
335 histograms as shown in Fig. 6.

336 The results exhibit noticeable differences in the pattern of cloud regimes over all study areas.
337 The diverse CF values are observed in winter and summer seasons for NPCs and PCs over
338 Karachi. In winter season, only stratus NPCs ($23 < \text{COT} < 60$, $800 > \text{CTP} > 680$ hPa) are
339 dominant with $\text{CF} \sim 0.9$. While, in summers, high value of $\text{CF} \sim 0.9$ for low and intermediate
340 thickness of high-level clouds such as Cirr-Stratus NPCs ($3.6 < \text{COT} < 23$, $180 < \text{CTP} < 440$
341 hPa) are observed. Similarly, the type of PCs in both summer and winter season that occurred
342 with $\text{CF} \sim 1.0$ include cirrus and cirr-stratus. The relatively reduced value of CF for thick NPCs
343 in winters and PCs in summers is attributed to the low values of AOD and high values of LTS.
344 The results depicted slight differences and similarities in CF values for thick and thin NPCs
345 respectively in winter season for all areas except Karachi. Besides, the high-level PCs are
346 identified in the two bins of CTP ($180 < \text{CTP} < 440$ hPa) and ($440 < \text{CTP} < 680$ hPa) over all
347 study areas. The formation of these similar types of PCs in winters are associated with the
348 similarities in Ω , LTS values and aerosols concentration.

349 Likewise, in summer season, the matrices of PCs and NPCs exhibit a wide range of cloud types.
350 However, the CF values are comparatively high for PCs. Most of the identified PCs are formed
351 in the two bins of CTP ($180 < \text{CTP} < 440$ hPa) and ($440 < \text{CTP} < 680$ hPa) with CF values
352 ranging from 0.8 to 1.0. The results suggest low values of CF for the low-lying thick NPCs
353 over all study areas. Moreover, the results illustrate a more frequent occurrence of all the three
354 types of thick NPCs in one bin of COT ($23 < \text{COT} < 60$) and all the three types of high-level
355 NPCs for CTP ($180 < \text{CTP} < 440$ hPa) over Delhi, Kanpur, and Gandhi College. Therefore,
356 these are considered the cloudiest regimes. Besides, contrasting regional variations are also
357 observed in PCs. The maximum CF values for all types of PCs are observed over Kanpur and
358 Gandhi College. Similarly, relatively good values of CF in a bin of COT ($23 < \text{COT} < 60$) and

359 a bin of CTP ($180 < \text{CTP} < 440$ hPa) over Lahore, Delhi, and Jaipur depict the frequent
 360 occurrence of thick and high-level PCs respectively. In addition, among all the estimated low-
 361 level PCs, cumulus and strato-cumulus exhibit good CF values (0.7) over Kanpur and Gandhi
 362 College. The formation of thick clouds can be attributed to the enhanced convection process
 363 due to the atmospheric instability.

364
 365

Table 3. Classification of clouds based on CTP – COT joint histograms.

CTP (hPa)	COT		
	0-3.6	3.6-23	23 to >60
440 to <180	Cirrus	Cirr-Stratus	Deep convection
680-440	Alto-Cumulus	Alto-Stratus	Nimbo-Stratus
<800 to 680	Cumulus	Strato-Cumulus	Stratus

366

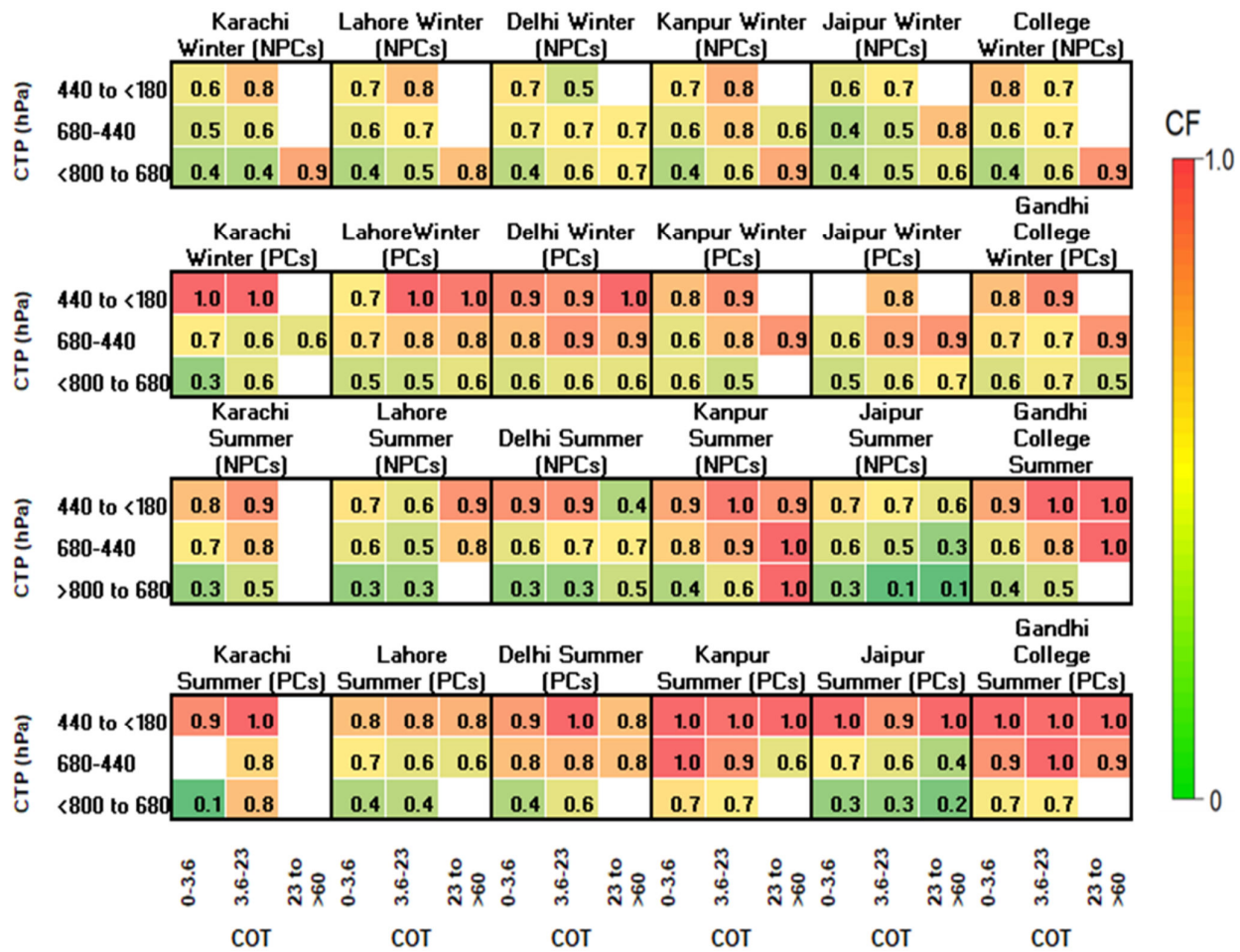


Figure 6. Types of NPCs and PCs in winter and summer season

367

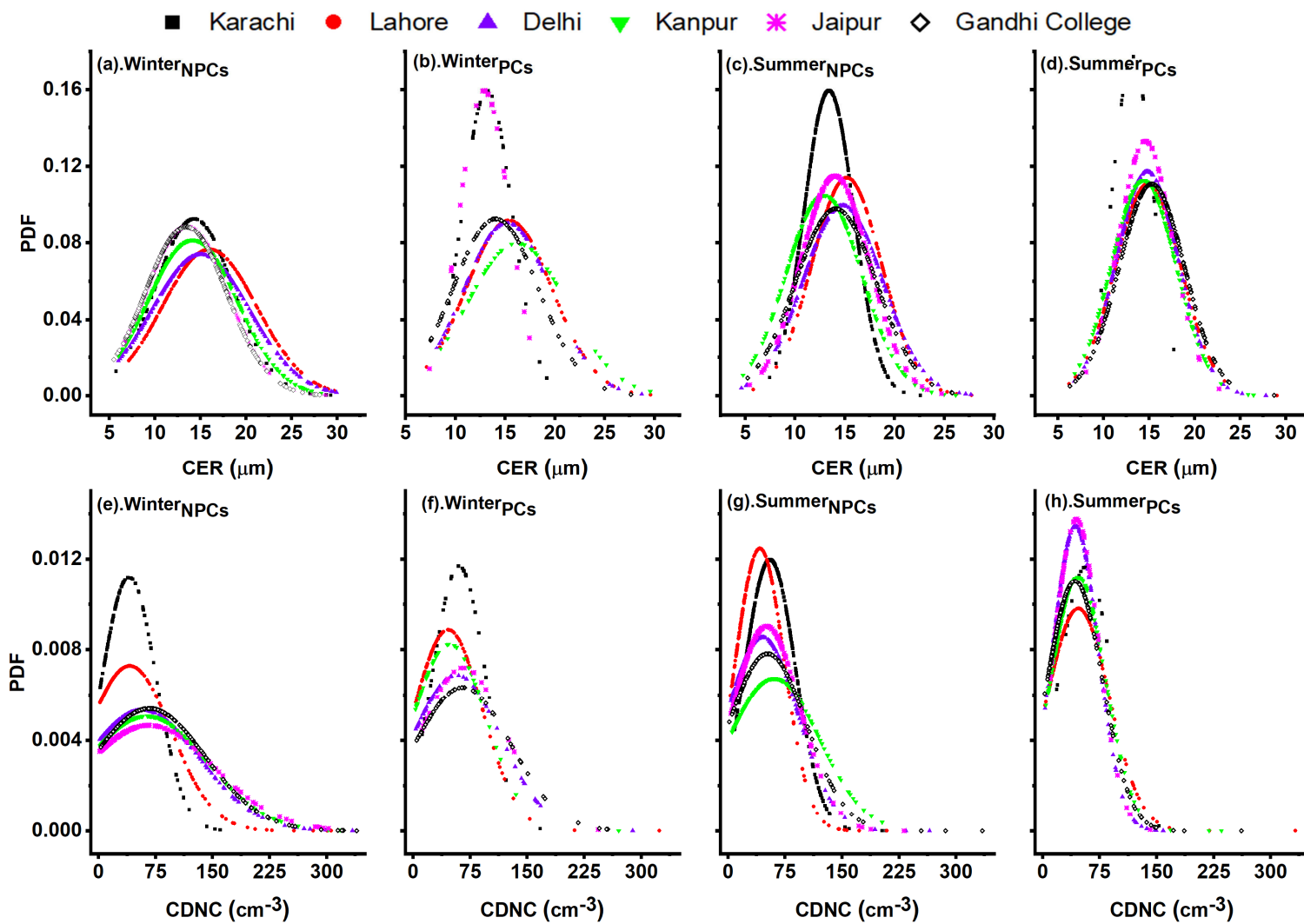
368

369 After estimating the cloud types, Fig. 7 shows the probability distribution function (PDF) of
370 cloud microphysical properties for the identification of differences in microstructure of NPCs
371 and PCs in summer and winter seasons. From the results it is depicted an approximately similar
372 pattern for the CER of NPCs in winter. However, the clouds have high peaks of PDF for lower
373 values of CDNC over Karachi. The low number of CDNC results in thin NPCs as shown in
374 Fig.7. Similarly, Fig. 7(c and g) shows the microstructure of NPCs in summer. The results
375 indicate that as compared to CER values in winter, the probability of CER $> \sim 15 \mu\text{m}$ is high in
376 summer season. However, high peak for CER $< 15 \mu\text{m}$ is observed over Karachi. Similarly, the
377 CDNC shows a high probability for CDNC $> 50 \text{ cm}^{-3}$ with the high PDF values over Karachi.
378 Where, the lowest number of CDNC is observed over Lahore indicating the formation of high-
379 level thin NPCs in summer.

380 Fig. 7(b and f) shows the distribution pattern of CER and CDNC of PCs in winter season. It is
381 clearly observed that the distribution of CER for PCs is like those for NPCs in winter season.
382 However, PDF have peak values for relatively higher CDNC, which illustrates the occurrence
383 of thick clouds. Fig. 7(d and h) shows the variations in CER and CDNC in summer season. The
384 results show a wider distribution for CER $> \sim 15 \mu\text{m}$ and higher peaks for CDNC $> \sim 50 \text{ cm}^{-3}$
385 suggesting the formation of thick PCs in summer as shown in Fig.6.

386

387



388

389

Figure 7. Probability density function (PDF) of precipitating (PCs) and non-precipitating clouds (NPCs) in winter and summer season

390 **3.4. Aerosol-Cloud-Precipitation Interaction (ACPI)**

391 In the following sections, ACPI is analyzed and discussed in detail for PCs and NPCs in
392 summer and winter seasons.

393 *3.4.1. Aerosol effects on cloud properties*

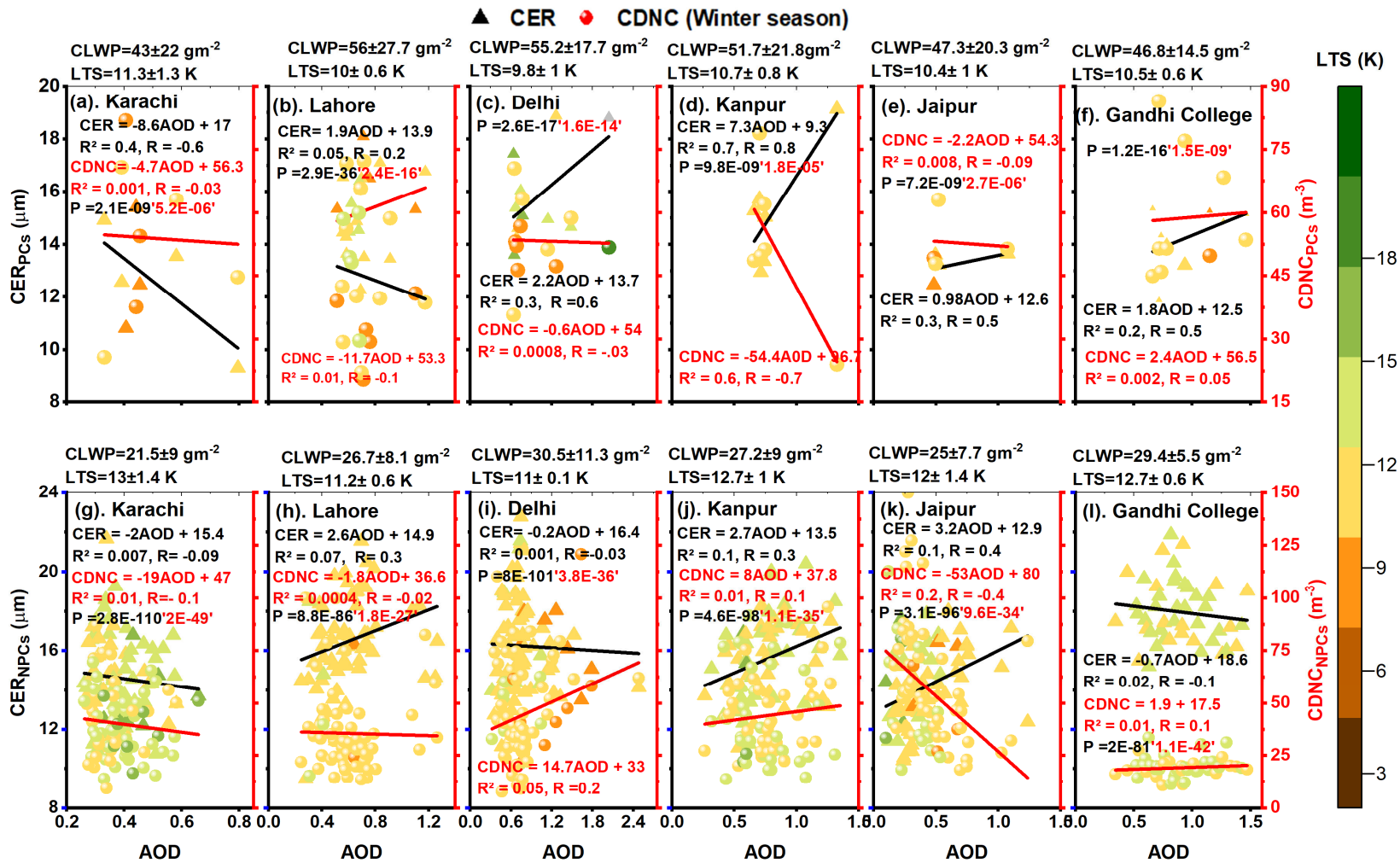
394 The impact of aerosols on CDNC and CER of PCs and NPCs is illustrated as scatter plots in
395 Fig. 8-9. The quantification of the AOD-CER and AOD-CDNC relationships is demonstrated
396 through detailed linear regressed slopes, regression coefficients (R^2) and Pearson's correlation
397 coefficient (R). The color bar represents the variations in LTS. **The results show that the two-**
398 **sample student's t test is carried out to analyze the AOD-CER and AOD-CDNC relationship in**
399 **view of statistics. The results illustrate that the relationships are statistically significant at 95%**
400 **($p < 0.05$) significance level for all study areas.** Fig.8 shows that in winter season, the AOD-
401 CER correlation is good for PCs and weak for NPCs. The results also show that the LTS values
402 are higher for NPCs. The weak AOD-CER correlation may be linked to the inhibition of droplet
403 growth due to less soluble aerosols, originated from biomass burning (Kang et al., 2015). In
404 our case, all the selected study areas are among the most urbanized and industrialized areas of
405 IGP. Therefore, most of the prevailing aerosols are the less soluble soot and BC particles. That
406 weakened activation of cloud droplets, inhibits the formation of PCs and evaporate to higher
407 altitudes and thereby increases the droplet residence time (Kumar & Physics, 2013). Besides,
408 the results show a contrasting pattern of LTS values. Although, RH over Karachi ($38.3 \pm 9\%$)
409 is higher than over the other study areas (shown in Table 2), the negative AOD-CER correlation
410 is observed over Karachi due to its coastal location, the low value of AOD and high level of
411 LTS.

412 Fig. 9 illustrates the AOD-CER and AOD-CDNC correlation in summer season. The results
413 depict a more significant and positive AOD-CER correlation in summer season than winter
414 season. Unlike winter season, the high LTS values are observed for PCs. Yuan(2008)
415 associated the positive AOD-CER correlation to the soluble organic aerosols. Myhre et al.
416 (2007) hypothesized that the positive AOD-CER correlation is a maximum for low CTP and
417 minimum for high CTP. Hence, in our study, referable to the approximated CF values shown
418 in Fig.6, the significant and positive AOD-CER correlation under unstable atmospheric
419 conditions resulted in thick and high-level clouds. Furthermore, it is observed that CER and
420 CDNC values for NPCs increase with increasing instability. Meanwhile, the enhanced process
421 of droplet activation may result in large AOD, higher CER, giant and fewer CCN (Yuan, 2008).

422 Therefore, the weak correlation of AOD with CER and CDNC may be due to the
423 anthropogenically ejected water-soluble organic aerosols and a smaller number of CCN.

424 Fig. 5S and 6S show the impact of AOD on CER and CDNC for PCs and NPCs in winter and
425 summer respectively. The results indicate a positive and weak AOD-CER correlation 0.2, 0.07
426 and 0.004 for NPCs over Kolkata, Dhaka and Patna respectively and for PCs (0.08) over both
427 Kolkata and Patna. Similarly, a positive and weak AOD-CDNC is observed over all areas for
428 PCs. Likewise, Fig. 6S also illustrates weak AOD-CER correlation is 0.06, 0.2 and 0.12 for
429 both types of clouds in summer. As compared to other areas, the correlation analysis is less
430 significant over Karachi, Kolkata, Dhaka and Patna. This can be attributed to the persistence
431 of diverse aerosol types influenced by their coastal locations, different meteorology and the
432 alternating inflow and outflow of easterly and westerly winds.

433 Recent advances in remote sensing led to cost-effective solutions and an increase in available
434 data at various temporal and spatial resolution to bridge scientific gaps among different
435 disciplines. While satellite-based retrievals have many advantages over in-situ and ground-
436 based measurement such as broader regional coverage and enhanced spatial resolution, they
437 are still prone to considerable uncertainties owing to the indirect nature of remote-sensing,
438 retrieval algorithms, thermal radiance, infrequency of satellite overpasses, and cloud top
439 reflectance (Hong et al., 2006; Tian et al., 2010; Hossain et al., 2006). In our study, apart from
440 the aforementioned factors contributing to the uncertainty, any residual cloud contamination
441 could also lead to biased retrieval of AOD. Likewise, satellite-based retrievals for cloud
442 properties are crucial to understanding the pivotal role of clouds in climate and the role of
443 clouds is still a dominant source of uncertainty in prediction of climate change. These,
444 uncertainties in AOD and retrievals of cloud properties also propagate through the modeling
445 process, potentially leading to less accurate climate predictions. Likewise, these uncertainties
446 appeared to influence the findings in the current investigation. For instance, a limited
447 correlation between AOD and CER is observed over Lahore, particularly in cloudier regimes
448 as depicted in Fig. (5-6). This contrasts with robust impacted documented in the earlier studies
449 (Michibata et al., 2014). However, high sensitivity of SIE is observed for PCs particularly in
450 winter season indicating the delay in onset of precipitation and more retention of clouds.



451

452 **Figure 8.** AOD-CER and AOD-CDNC regression and correlation coefficient considered at 95% confidence level for PCs and NPCs over all
 453 study areas in winter season.

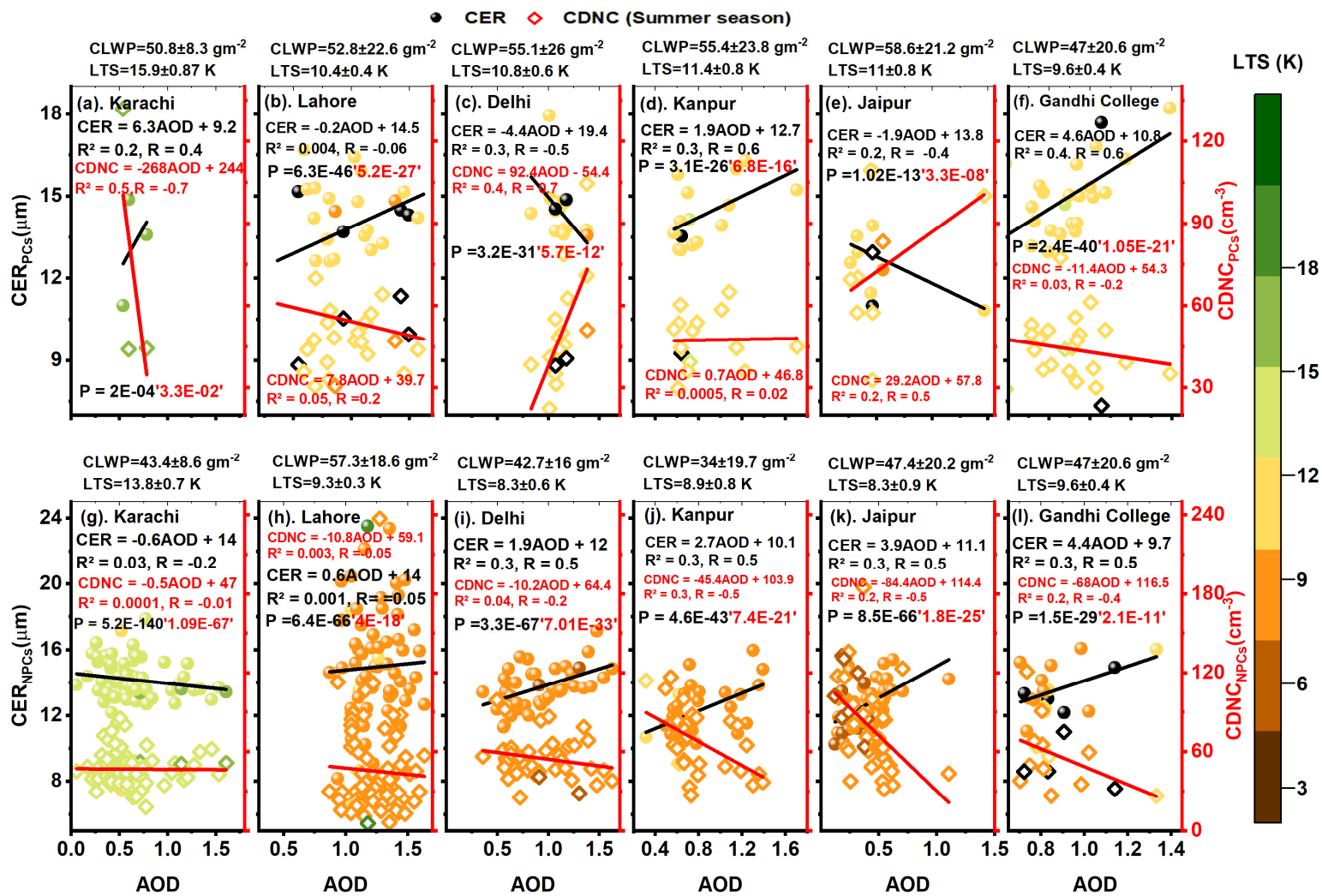


Figure 9. Same as Fig. 8 but in summer season.

454

455

3.4.2. Seasonal variations in sensitivities of aerosol-cloud indirect effects and ACI

456
457 Fig.10 shows assessment of four ACI sensitivities in terms of CDNC using daily mean values
458 of MODIS observations available over the entire study area. Since, studying the effects of
459 aerosols on the co-located clouds is a challenging task due to the overestimation of thin clouds
460 in AOD retrievals. Therefore, to minimize the propagation of AOD retrieval errors in ACI, the
461 current study attempted to estimate the sensitivities of different cloud mechanisms to CDNC.

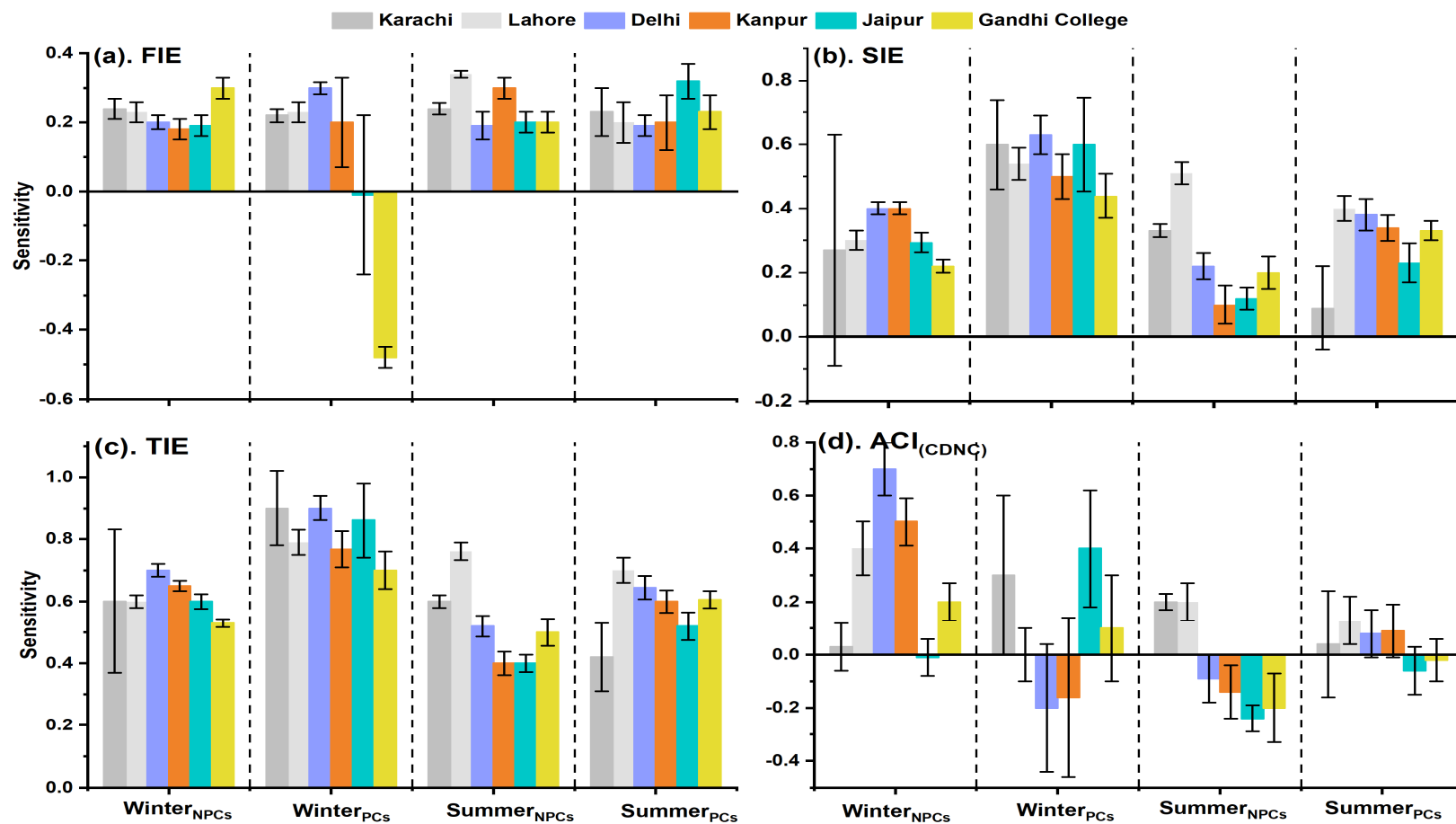
462 The sensitivity of CER to CDNC is assessed as a signature of FIE as shown in Fig.10a. The
463 positive values illustrate that CER decreases with an increase in CDNC revealing the
464 occurrence of the Twomey effect. Whilst the negative values depict the anti-Twomey effect.
465 Tripathi et al., (2007) divided IGP into four regions as western, central, eastern part of IGP and
466 the foothills of Himalayas. Their results depicted high concentration of dust in western part,
467 and an increase in anthropogenic aerosols as one moves from western to eastern part of IGP.
468 Therefore, they attributed the resulted strong indirect effect in winter to the high concentration
469 of regional anthropogenic pollution. However, in our case, the FIE is investigated for both PCs
470 and NPCs in both seasons. The resulted approximations in winter season show strong (weak)
471 sensitivity of FIE for PCs (NPCs). Similarly, the estimated sensitivity of FIE for all NPCs and
472 PCs is also positive in the summer season. Fig. 7S(a) shows sensitivities for FIE in both seasons
473 for PCs and NPCs. The results indicate high values of sensitivity FIE in winter season which
474 is similar to the results for Karachi, Lahore, Delhi and Kanpur as shown in Fig. 10 a. This is
475 attributed to high level of aerosol emission from residential heating and industrial activities.
476 Furthermore, the results illustrate higher values of FIE in summer. This is attributed to the
477 massive aerosol loading due to aerosol carried by winds and originated by anthropogenic
478 activities and unstable meteorology.

479 Fig. 10b illustrates the sensitivity of CLWP to CDNC as a proxy for evaluation of the SIE or
480 lifetime effect. The positive sensitivity estimated for all NPCs and PCs suggested that the
481 CLWP increase with increase in aerosol. Further, the results show that the sensitivity of SIE is
482 stronger for PCs in winter which indicate the delay in onset of high PR. Similarly, the results
483 show that the SIE sensitivity values are higher for PCs than for NPCs in the corresponding
484 seasons. Therefore, the results depict that the lifetime of PCs is greater than NPCs. Which is
485 attributed to the high level of RH for PCs as shown in Table 2. Fig. 10 (a and b) shows that the
486 FIE sensitivities are weaker than SIE.

487 Fig. 10c shows the TIE in terms of the sensitivity of COT to CDNC. The results illustrate
488 positive values of sensitivity for all NPCs and PCs which indicate that COT increases with
489 increase in aerosol concentration. The results also reveal that sensitivity of TIE is a linear sum
490 of the sensitivities of FIE and SIE. Further, the results also suggest that the variations in TIE
491 sensitivity are largely dependent on SIE.

492 Fig.10d shows the sensitivity of CDNC to AOD as an estimation of ACI in terms of CDNC.
493 The positive values show the increase in CDNC with the increase in AOD. Therefore, positive
494 ACI reflects the inhibition of precipitation formation. Whilst, the negative values illustrate the
495 decrease in CDNC and enhanced PR (Fan et al., 2018). The results depicted relatively large
496 and positive sensitivities for NPCs in winter over Lahore, Delhi, and Kanpur, which inhibits
497 the onset of rainfall. The Sensitivity of ACI for NPCs in summer is positive over Karachi and
498 Lahore and negative over Delhi, Kanpur, Jaipur, and Gandhi College. Ackerman et al. (2004)
499 associated the negative ACI_{CDNC} to the wet scavenging and mixing of air by entrainment. In
500 our case, negative ACI may be due to the growth of CER and decrease in CDNC with aerosol
501 loading under unstable conditions (shown in Fig. 9). Further, the magnitude of sensitivity for
502 PCs in summer is low. Which can be due to the droplet growth through collision coalescence
503 and wet scavenging in thick clouds, decreased dependency on CCN.

504



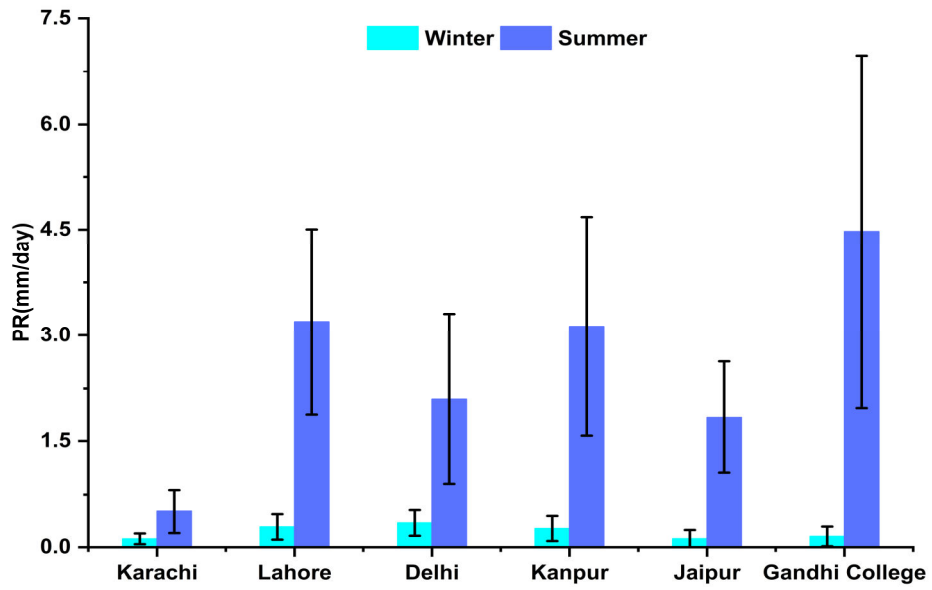
506

507 **Fig. 10.** The sensitivity metrics estimated for aerosol-cloud relationship using CDNC is shown in (a) $FIE = -\left(\frac{\partial \ln(CER)}{\partial \ln(CDNC)}\right)$ (b) $SIE = \left(\frac{\partial \ln(cLWP)}{\partial \ln(CDNC)}\right)$,
 508 (c) $TIE = \left(\frac{\partial \ln(COT)}{\partial \ln(CDNC)}\right)$ and (d) $ACI = \left(\frac{\partial \ln(CDNC)}{\partial \ln(AOD)}\right)$. Where, the error bars show the standard deviation (SD).

509 3.4.3. *Aerosol effects on precipitation*

510 Fig. 11 shows the average values of PR in mm/day retrieved from TRMM. The results show
511 an obvious seasonal difference in precipitation occurrence. The reason for the high (low) PR
512 values is due to the suitable meteorological condition including high (low) LTS values for PCs
513 in summer (winter) season (shown in Fig. 8-9). The stable atmospheric condition with high
514 LTS value in winter serves to inhibit the convection process and have a significant impact on
515 controlling the PR in winter (Zhao et al., 2006). Conversely, during summer season, the
516 meteorological instability prevails with low LTS values which result in high RH. This not only
517 causes enhanced AOD due to the water uptake and resulted swelled hydrophilic aerosols (Alam
518 et al., 2010; Alam et al., 2011) but also affects the cloud and precipitation formation due to the
519 enhanced evaporation and convection. Additionally, Fig. 8-9 also show evidently and
520 specifically during summer that the possible cause of positive AOD-CER correlation is the
521 negative AOD-CDNC correlation under unstable meteorology over all areas except Karachi.
522 As a result, Fig. 11 shows high (low) values of PR over all areas with maximum over Gandhi
523 College (Karachi). The results show high (low) approximation of PR over Gandhi College
524 (Karachi). Knowing that the rate of conversion of CDNC to precipitation is proportional to
525 CER (Wolf & Toon, 2014). Therefore, the high PR values is due to the growth of bigger cloud
526 droplets in summers. Further, apart from the reasons mentioned in the preceding sections, the
527 other justification for the differently perturbed aerosols, clouds and precipitation pattern over
528 the study areas in summers is due to the entrance of southeast winds from Bay of Bengal
529 passing across Gandhi College to Delhi and Lahore and entrance of same winds from Arabian
530 sea to Pakistan through Karachi (Anwar et al., 2022).

531 Fig. 12 shows scatter plots of PR verses CDNC. The plot is colored with COT to examine the
532 impact of CDNC on PR for similar macrophysics. When CDNC are few, then the COT are
533 sparse that grow larger, form less reflective clouds and precipitate faster (Kump & Pollard,
534 2008). The same phenomenon seems true in our case. The results illustrate high PR (0.0007
535 mm/day) values for clouds with COT ranging from 3 to 28 with CDNC < $\sim 50 \text{ cm}^{-3}$ and
536 intermediate for optically thick clouds and CDNC > $\sim 50 \text{ cm}^{-3}$ in both seasons.

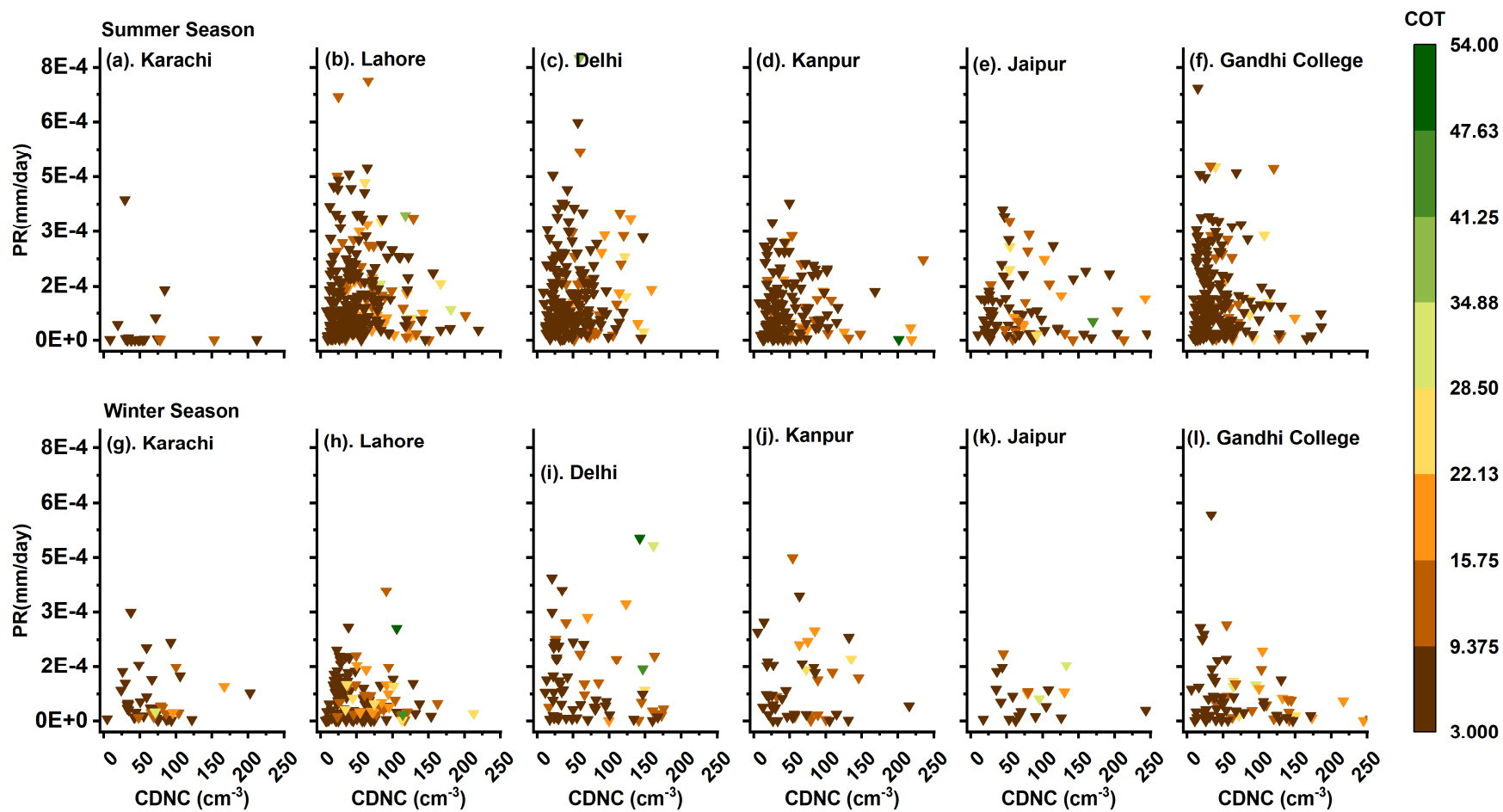


537

538

539

Figure 11. Mean Precipitation rate (PR) for the PCs in winter and summer season and SD values with 95% confidence interval.



540

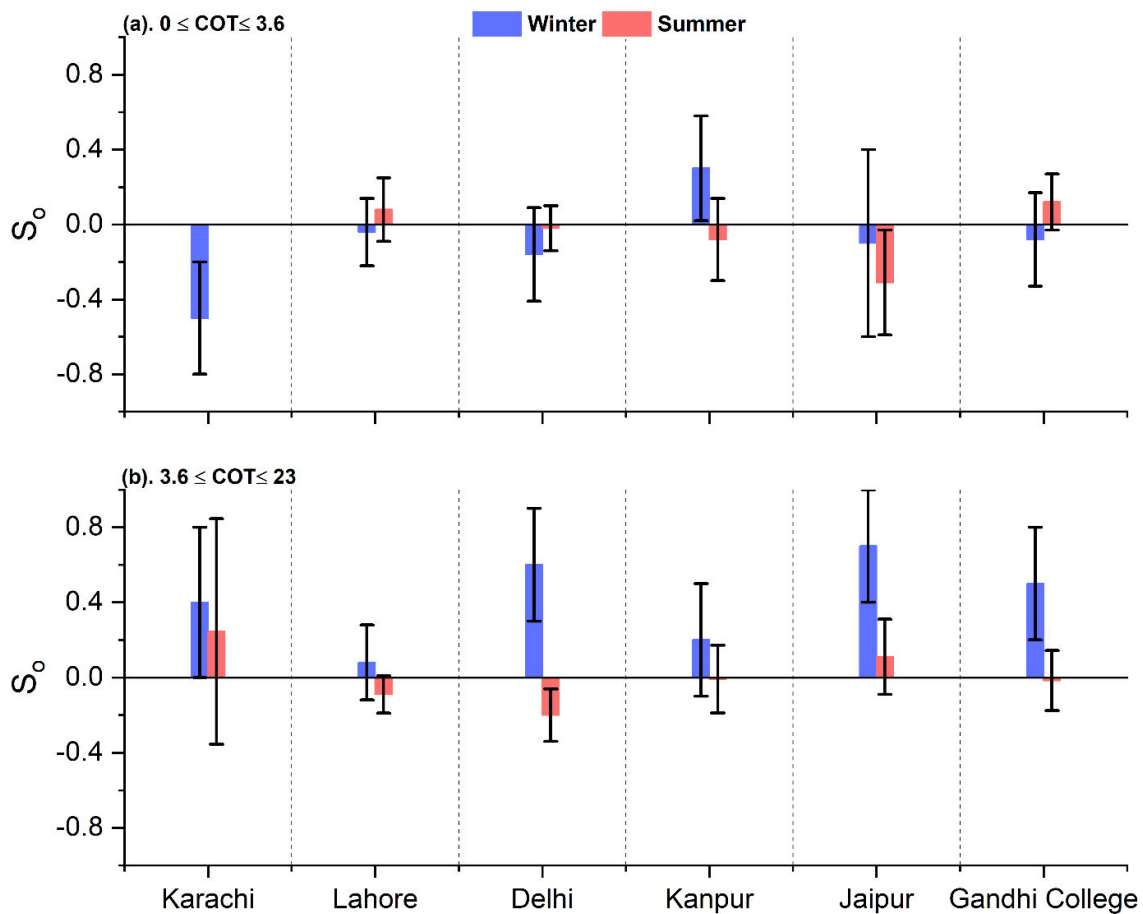
541

Figure 12. Scatter diagrams of PR (mm/day) versus CDNC (cm⁻³) in summer and winter seasons. color coding shows the COT of PCs.

542

543 Fig.13 shows the sensitivity (S_o) of PR to CDNC defined by $S_o = \left(-\frac{d\ln(PR)}{d\ln(CDNC)}\right)_{COT}$ for clouds
 544 of low and intermediate thickness illustrated in Fig. 13 a and Fig. 13 b respectively. However,
 545 sensitivity analysis for $COT > 23$ could not be performed due to less number (0 to 04) of
 546 available samples. In the sensitivity equation the minus sign shows the suppression of
 547 precipitation formation due to the increase in CDNC. Further, when S_o is positive, correlation
 548 between PR and CDNC is negative; however, for negative S_o , PR and CDNC are positively
 549 correlated. The results show peak values of S_o i.e., 0.7 ± 0.3 , 0.6 ± 0.3 , 0.5 ± 0.3 , and $0.4 \pm$
 550 0.4 over Jaipur, Delhi, Gandhi College and Karachi respectively at intermediate values of COT
 551 in winter, indicating the occurrence of lightly precipitating clouds. Referable to Fig. 13b, the
 552 low magnitude of S_o 0.2 ± 0.3 and 0.08 ± 0.2 over Kanpur and Lahore respectively is due to
 553 coagulation, in which precipitations are less sensitive to CDNC.

554



555

556 **Figure 133.** Sensitivity 'So' of precipitation rate (PR) for two bins of COT shown in (a). $0 \leq$
 557 $COT \leq 3.6$ and (b). $3.6 \leq COT \leq 23$.

558

559 **4. Conclusion**

560 In this study, the long-term (2001-2021) data retrievals from MODIS coupled with TRMM and
561 NCEP/NCAR reanalysis-II datasets over the entire study area are compiled and analyzed for
562 PCs and NPCs in winter and summer season. The following are the main findings of this study.

563 A decadal decrease in AOD is observed over Karachi (-1.9%) and Jaipur (-0.5%). Meanwhile,
564 AOD exhibits an increase over Lahore (5.2%), Delhi (9%), Kanpur (10.7%) and Gandhi
565 College (22.7%). The LTS values are High (low) for NPCs (PCs) in winter and for PCs (NPCs)
566 in summer season. However, among all study areas, Karachi exhibits comparatively high LTS
567 values in both seasons. Apart, the increase in RH% for PCs ranged from 33-57% in winter and
568 from 25-45 % in summer. $\Omega > 0$ for all NPCs in winter and < 0 for PCs in both winter and
569 summer seasons.

570 In winter season low frequency of cloudy days over Karachi and high over Lahore and Gandhi
571 College is estimated. Also, the high number of PCs are estimated only over Lahore. In summer
572 season, out of the 74 % of the cloudy days , 60 % are PCs over Gandhi College. Similarly, most
573 of the clouds over Lahore, Delhi and Jaipur are PCs. Conversely, the least number of PCs (6
574 %) is found over Karachi. The high-level PCs are identified in one bin of CTP ($180 < CTP <$
575 440 hPa) over all study areas in winters. In summer season, all the three types of high level and
576 thick PCs have significant values of CF. The low-level PCs are identified as stratus clouds.
577 Further, PDF values for $CER > \sim 15 \mu m$ and $CDNC > \sim 50 cm^{-3}$ for NPCs and PCs is high
578 (low) in summer (winter) over all areas except Karachi.

579 The AOD-CER correlation is good for PCs and weak for NPCs in winter season. Also, the CER
580 and CDNC values increase with increase in LTS. The sensitivity value of FIE is high (low) for
581 PCs (NPCs) in winter. Further, magnitude of sensitivity of FIE (SIE) is low (high). Also, the
582 sensitivity of TIE is a linear sum of the sensitivities of FIE and SIE. Further, ACI sensitivity
583 values for PCs in summer are small, illustrating less dependency of CER on CDNC in thick
584 clouds.

585 The high (low) PR values are observed in summer (winter). Further, high PR values for
586 comparatively thin clouds with fewer $CDNC < \sim 50 cm^{-3}$ and intermediate for optically thick
587 clouds and $CDNC > \sim 50 cm^{-3}$ are observed. Sensitivity values are small (high) for thick clouds
588 in summer (winter).

589 Being one of the major source regions of anthropogenic aerosols across the globe, IGP
590 offers interesting insights into the study of ACPI coupled with aerosol indirect effects. This
591 study highlights that the aerosol-cloud relationship exhibits different behavior under
592 different meteorological conditions, at coastal and inland locations. Thus, compared to
593 other study areas, the stable atmospheric conditions due to the constant sea breeze
594 weakened the ACI over Karachi, which resulted in a smaller number of CDNC, NPCs, and
595 PCs. Further, our study also provides a very good platform for the detailed analysis of
596 sensitivity tests of aerosol indirect effects and precipitation formation.

597 **Limitations and future recommendations:**

598 Although the current study is as thorough as possible, however, it has its limitations due to
599 the topographical complexity of IGP, the lack of in-situ measuring instruments in Pakistan,
600 and the intrinsic uncertainties associated with satellite-based data. Therefore, simulations
601 of ground-based measurements along with satellite-based retrievals and calculation of
602 cloud properties and CCN by different Community Atmosphere Model (CAM) and
603 Weather Research and Forecasting (WRF) Models are recommended for deep insight into
604 the various mechanisms of ACPI over IGP.

605 **Data Availability:** The MODIS and TRMM data can be obtained from the NASA Goddard
606 Earth Sciences Data and Information Center (GES DISC) and can be retrieved from the
607 websites: <https://modis.gsfc.nasa.gov/data/> and <https://gpm.nasa.gov/data> . The reanalysis-
608 II datasets are obtained from the website:
609 <https://psl.noaa.gov/data/gridded/data.ncep.reanalysis2.html> . The processed data used in
610 this work are available on reasonable request from the corresponding author.

611 **Author contribution:** NG processed and analyzed the data and wrote the original draft of
612 the manuscript. KA proposed the Idea, supervised this work and revised the manuscript.
613 YL helped in revising the manuscript.

614 **Acknowledgment:** The authors gratefully acknowledge the NASA Goddard Earth
615 Sciences Data and Information Services Center (GES DISC) for the provision of freely
616 available data retrieved from MODIS and TRMM. We are also grateful to the NOAA
617 Physical Sciences Laboratory (PSL) for free accessibility to (NCEP/NCAR) reanalysis-II
618 datasets.

619

620

621 **References**

- 622 Ackerman, A. S., Kirkpatrick, M. P., Stevens, D. E., & Toon, O. B.: The impact of humidity above stratiform
623 clouds on indirect aerosol climate forcing, *Nature.*, *432*, 1014-1017,
624 <https://doi.org/10.1038/nature03174> , 2004.
- 625 Alam, K., Iqbal, M. J., Blaschke, T., Qureshi, S., & Khan, G.: Monitoring spatio-temporal variations in aerosols
626 and aerosol–cloud interactions over Pakistan using MODIS data, *Adva. Space Res.*, *46*, 1162-1176,
627 <https://doi.org/10.1016/j.asr.2010.06.025> , 2010.
- 628 Alam, K., Qureshi, S., & Blaschke, T.: Monitoring spatio-temporal aerosol patterns over Pakistan based on
629 MODIS, TOMS and MISR satellite data and a HYSPLIT model, *Atmos. Envi.*, *45*, 4641-4651,
630 <https://doi.org/10.1016/j.atmosenv.2011.05.055> , 2011.
- 631 Albrecht, B. A.: Aerosols, cloud microphysics, and fractional cloudiness, *Sci.*, *245*, 1227-1230,
632 <https://doi.org/10.1126/science.245.4923.122> , 1989.
- 633 Ali, G., Bao, Y., Ullah, W., Ullah, S., Guan, Q., Liu, X., . . . Ma, J.: Spatiotemporal trends of aerosols over
634 urban regions in Pakistan and their possible links to meteorological parameters, *Atmo.*, *11*, 306,
635 <https://doi.org/10.3390/atmos11030306> , 2020.
- 636 Andreae, M., & Rosenfeld, D.: Aerosol–cloud–precipitation interactions. Part 1. The nature and sources of
637 cloud-active aerosols, *Earth. Sci. Rev.*, *89*, 13-41, <https://doi.org/10.1016/j.earscirev.2008.03.001> ,
638 2008.
- 639 Anttila, T., Brus, D., Jaatinen, A., Hyvärinen, A. P., Kivekäs, N., Romakkaniemi, S., ... & Lihavainen, H.:
640 Relationships between particles, cloud condensation nuclei and cloud droplet activation during the third
641 Pallas Cloud Experiment, *Atmos. Chem. Phys.*, *12*, 11435-11450, [https://doi.org/10.5194/acp-12-11435-](https://doi.org/10.5194/acp-12-11435-2012)
642 [2012](https://doi.org/10.5194/acp-12-11435-2012) , 2012.
- 643 Anwar, K., Alam, K., Liu, Y., Huang, Z., Huang, J., & Liu, Y.: Analysis of aerosol cloud interactions with a
644 consistent signal of meteorology and other influencing parameters, *Atmos. Res.*, *275*, 106241,
645 <https://doi.org/10.1016/j.atmosres.2022.106241> , 2022.
- 646 Brenguier, J.-L., Pawlowska, H., Schüller, L., Preusker, R., Fischer, J., & Fouquart, Y.: Radiative properties of
647 boundary layer clouds: Droplet effective radius versus number concentration, *Atmos. Sci.*, *57*, 803-
648 821, [https://doi.org/10.1175/1520-0469\(2000\)057<0803:RPOBLC>2.0.CO;2](https://doi.org/10.1175/1520-0469(2000)057<0803:RPOBLC>2.0.CO;2) , 2000.
- 649 Chen, F., Sheng, S., Bao, Z., Wen, H., Hua, L., Paul, N. J., & Fu, Y. : Precipitation Clouds Delineation Scheme
650 in Tropical Cyclones and Its Validation Using Precipitation and Cloud Parameter Datasets from
651 TRMM, *Applied Met. Climatology.* *57*, 821-836, <https://doi.org/10.1175/JAMC-D-17-0157.1> , 2018.
- 652 Chen, Q., Yin, Y., Jin, L.-j., Xiao, H., & Zhu, S.: The effect of aerosol layers on convective cloud microphysics
653 and precipitation, *Atmos. Res.*, *101*, 327-340, <https://doi.org/10.1016/j.atmosres.2011.03.007> , 2011
- 654 Costantino, L., & Bréon, F.: Analysis of aerosol-cloud interaction from multi-sensor satellite observations,
655 *Atmos. Sci.*, *37*, <https://doi.org/10.1029/2009GL041828> , 2010
- 656 Fan, C., Ding, M., Wu, P., & Fan, Y.: The Relationship between Precipitation and Aerosol: Evidence from
657 Satellite Observation, *Atmos. Oce. Phy.*, <https://doi.org/10.48550/arXiv.1812.02036> , 2018.
- 658 Feingold, G., Eberhard, W. L., Veron, D. E., & Previdi, M.: First measurements of the Twomey indirect effect
659 using ground-based remote sensors, *Geophy. Res. Let.*, *30*, <https://doi.org/10.1029/2002GL016633> ,
660 2003.
- 661 Gryspeerdt, E., Quaas, J., & Bellouin, N.: Constraining the aerosol influence on cloud fraction, *JGR. Atmos.*, *121*,
662 3566-3583, <https://doi.org/10.1002/2015JD023744> , 2016.
- 663 Hassan, M. A., Mehmood, T., Liu, J., Luo, X., Li, X., Tanveer, M., & Abid, M.: A review of particulate pollution
664 over Himalaya region: Characteristics and salient factors contributing ambient PM pollution. *Atmos.*
665 *Envi.*, *294*, 119472, <https://doi.org/10.1016/j.atmosenv.2022.119472> , 2022.
- 666 Hong, Y., Hsu, K. L., Moradkhani, H., & Sorooshian, S.: Uncertainty quantification of satellite precipitation
667 estimation and Monte Carlo assessment of the error propagation into hydrologic response, *Wat. Resc.*
668 *Res.*, *42*, 8, <https://doi.org/10.1029/2005WR004398> , 2006.
- 669 Hossain, F., Anagnostou, E. N., & Bagtzoglou, A.: On Latin Hypercube sampling for efficient uncertainty
670 estimation of satellite rainfall observations in flood prediction, *Comp. & geosc.*, *32*, 6, 776-792,
671 <https://doi.org/10.1016/j.cageo.2005.10.006> , 2006.
- 672 Jiang, H., Feingold, G., & Cotton, W.: Simulations of aerosol-cloud-dynamical feedbacks resulting from
673 entrainment of aerosol into the marine boundary layer during the Atlantic Stratocumulus Transition
674 Experiment, *JGR. Atmos.*, *107*, AAC 20-1-AAC 20-11, <https://doi.org/10.1029/2001JD001502> , 2002.
- 675 Jung, E.: Aerosol-cloud-precipitation interactions in the trade wind boundary layer, Ph.D Thesis, Meteorology
676 and Physical Oceanography, University of Miami, 91-pp., 2012.
- 677 Kang, N., Kumar, K. R., Yin, Y., Diao, Y., Yu, X.: Correlation analysis between AOD and cloud parameters to
678 study their relationship over China using MODIS data (2003-2013): impact on cloud formation and
679 climate change, *AAQR.*, *15*, 958-973, <https://doi.org/10.4209/aaqr.2014.08.0168> , 2015.

680 Kaskaoutis, D., Kumar Kharol, S., Sinha, P., Singh, R., Kambezidis, H., Rani Sharma, A.: Extremely large
681 anthropogenic-aerosol contribution to total aerosol load over the Bay of Bengal during winter season,
682 *Atmos. Chem. Phys.*, *11*, 7097-7117, <https://doi.org/10.5194/acp-11-7097-2011>, 2011.

683 Kedia, S., Ramachandran, S., Holben, B., & Tripathi, S.: Quantification of aerosol type, and sources of aerosols
684 over the Indo-Gangetic Plain, *Atmos. Environ.*, *98*, 607-
685 619, <https://doi.org/10.1016/j.atmosenv.2014.09.022>, 2014.

686 Koike, M., Asano, N., Nakamura, H., Sakai, S., Nagao, T., & Nakajima, T.: Modulations of aerosol impacts on
687 cloud microphysics induced by the warm Kuroshio Current under the East Asian winter monsoon, *JGR*.
688 *Atmos.*, *121*, 282-297, <https://doi.org/10.1002/2016JD025375>, 2016.

689 Kubar, T., Hartmann, D., & Wood, R.: Understanding the importance of microphysics and macrophysics for
690 warm rain in marine low clouds. Part I: Satellite observations, *Atmos. Sci.* *66*, 2953-2972,
691 <https://doi.org/10.1175/2009jas3071.1>, 2009.

692 Kumar, A., & Physics, S.: Variability of aerosol optical depth and cloud parameters over North Eastern regions
693 of India retrieved from MODIS satellite data, *Atmos. Sol. Terr. Phys.*, *100*, 34-
694 49, <https://doi.org/10.1016/j.jastp.2013.03.025>, 2013.

695 Kump, L. R., & Pollard, D.: Amplification of Cretaceous Warmth by Biological Cloud Feedbacks, *Sci.*, *320*,
696 195-195, <https://doi.org/10.1126/science.1153883>, 2008.

697 Li, J., Lv, Q., Zhang, M., Wang, T., Kawamoto, K., Chen, S., & Zhang, B.: Effects of atmospheric dynamics and
698 aerosols on the fraction of supercooled water clouds, *Atmos. Chem. Phys.*, *17*, 1847-
699 1863, <https://doi.org/10.5194/acp-17-1847-2017>, 2017.

700 López-Romero, J., Montávez, J., Jerez, S., Lorente-Plazas, R., Palacios-Peña, L., & Jiménez-Guerrero, P.:
701 Precipitation response to aerosol–radiation and aerosol–cloud interactions in regional climate
702 simulations over Europe. *Atmos. Chem. Phys.*, *21*, 415-430, <https://doi.org/10.5194/acp-21-415-2021>,
703 2021.

704 Masmoudi, M., Chaabane, M., Tanré, D., Gouloup, P., Blarel, L., & Elleuch, F.: Spatial and temporal variability
705 of aerosol: size distribution and optical properties, *Atmos. Res.*, *66*, 1-
706 19, [https://doi.org/10.1016/S0169-8095\(02\)00174-6](https://doi.org/10.1016/S0169-8095(02)00174-6), 2003.

707 McCoy, D., Field, P., Schmidt, A., Grosvenor, D., Bender, F., Shipway, B., & Elsaesser, G.: Aerosol midlatitude
708 cyclone indirect effects in observations and high-resolution simulations, *Atmos. Chem. Phys.*, *18*, 5821-
709 5846, <https://doi.org/10.5194/acp-18-5821-2018>, 2018.

710 Michibata, T., Kawamoto, K., & Takemura, T.: The effects of aerosols on water cloud microphysics and
711 macrophysics based on satellite observations over East Asia and the North Pacific, *Atmos. Chem. Phys.*,
712 *14*, 10515-10541, <https://doi.org/10.5194/acp-14-11935-2014>, 2014.

713 Myhre, G., Stordal, F., Johnsrud, M., Kaufman, Y., Rosenfeld, D., Storelvmo, T.: Aerosol-cloud interaction
714 inferred from MODIS satellite data and global aerosol models, *Atmos. Chem. Phys.*, *7*, 3081-3101,
715 <https://doi.org/10.5194/acp-7-3081-2007>, 2007.

716 Nair, V., Giorgi, F., Keshav Hasyagar, U.: Amplification of South Asian haze by water vapour–aerosol
717 interactions, *Atmos. Chem. Phys.*, *20*, 14457-14471, <https://doi.org/10.5194/acp-20-14457-2020>, 2020.

718 Naud, C., Posselt, D., & van den Heever, S.: Observed covariations of aerosol optical depth and cloud cover in
719 extratropical cyclones, *JGR: Atmos.*, *122*, 10-338, <https://doi.org/10.1002/2017JD027240>, 2017.

720 Rossow, W., & Schiffer, R.: Advances in understanding clouds from ISCCP, *Bul. Amer. Meteor. Soci.*, *80*,
721 2261-2288, [https://doi.org/10.1175/15200477\(1999\)080<2261:AIUCFI>2.0.CO;2](https://doi.org/10.1175/15200477(1999)080<2261:AIUCFI>2.0.CO;2), 1999.

722 Sharma, P., Ganguly, D., Sharma, A., Kant, S., Mishra, S.: Assessing the aerosols, clouds and their relationship
723 over the northern Bay of Bengal using a global climate model, *Earth. Spac. Sci.*, *10*, e2022EA002706,
724 <https://doi.org/10.1029/2022EA002706>, 2023.

725 Sherwood, S., Roca, R., Weckwerth, T., & Andronova, N.: Tropospheric water vapor, convection, and climate,
726 *Rev. of Geophys. (AGU)*, *48*, 2, <https://doi.org/10.1029/2009RG000301>, 2010.

727 Singh, A., Rastogi, N., Sharma, D., Singh, D.: Inter and intra-annual variability in aerosol characteristics over
728 northwestern Indo-Gangetic Plain, *AAQR.*, *15*, 376-386, <https://doi.org/10.4209/aaqr.2014.04.0080>,
729 2015.

730 Srivastava, P., Pal, D., Aruche, K., Wani, S., & Sahrawat, K.: Soils of the Indo-Gangetic Plains: a pedogenic
731 response to landscape stability, climatic variability and anthropogenic activity during the Holocene,
732 *Earth. Sci. Rev.*, *140*, 54-71, <https://doi.org/10.1016/j.earscirev.2014.10.010>, 2015.

733 Stevens, B., & Feingold, G.: Untangling aerosol effects on clouds and precipitation in a buffered system,
734 *Nature*, *461*, 607-613, <https://doi.org/10.1038/nature08281>, 2009.

735 Sun, J., & Ariya, P.: Atmospheric organic and bio-aerosols as cloud condensation nuclei (CCN): A review,
736 *Atmos. Environ.*, *40*, 795-820, <https://doi.org/10.1016/j.atmosenv.2005.05.052>, 2006.

737 Tao, W., Chen, J., Li, Z., Wang, C., & Zhang, C.: Impact of aerosols on convective clouds and precipitation,
738 *Rev. Geophys.*, *50*, <https://doi.org/10.1029/2011RG000369>, 2012.

739 Thomas, A., Kanawade, V., Sarangi, C., & Srivastava, A.: Effect of COVID-19 shutdown on aerosol direct
740 radiative forcing over the Indo-Gangetic Plain outflow region of the Bay of Bengal, *Sci. Total Envi.*,
741 782, 146918, <https://doi.org/10.1016/j.scitotenv.2021.146918>, 2021.

742 Tian, Y., & Peters-Lidard, C.: A global map of uncertainties in satellite-based precipitation
743 measurements, *Geophys. Res. Let.*, 37, 24, <https://doi.org/10.1029/2010GL046008>, 2010.

744 Tripathi, S. N., Pattnaik, A., & Dey, S.: Aerosol indirect effect over Indo-Gangetic plain, *Atmos. Envi.*, 41, 33,
745 7037-7047, <https://doi.org/10.1016/j.atmosenv.2007.05.007>, 2007.

746 Twomey, S.: The influence of pollution on the shortwave albedo of clouds, *Atmos. Sci.*, 34, 1149-
747 1152, [https://doi.org/10.1175/1520-0469\(1977\)034<1149:TIOPOT>2.0.CO;2](https://doi.org/10.1175/1520-0469(1977)034<1149:TIOPOT>2.0.CO;2), 1977.

748 Verma, S., Ramana, M., & Kumar, R.: Atmospheric rivers fueling the intensification of fog and haze over Indo-
749 Gangetic Plains, *Sci. Reports.*, *Nature*, 12, 5139, 2022.

750 Wolf, E., & Toon, O.: Controls on the Archean climate system investigated with a global climate model,
751 *Astrobiology*, 14, 241-253, <https://doi.org/10.1089/ast.2013.1112>, 2014.

752 Wood, R.: Relationships between optical depth, liquid water path, droplet concentration, and effective radius in
753 adiabatic layer cloud, University of Washington, 3, 2006.

754 Wu, P., Dong, X., Xi, B., Liu, Y., Thieman, M., & Minnis, P.: Effects of environment forcing on marine
755 boundary layer cloud-drizzle processes, *JGR: Atmos.*, 122, 4463-
756 4478, <https://doi.org/10.1002/2016JD026326>, 2017.

757 Wyant, M., Bretherton, C., Bacmeister, J., Kiehl, J., Held, I., Zhao, M., Soden, B.: A comparison of low-latitude
758 cloud properties and their response to climate change in three AGCMs sorted into regimes using mid-
759 tropospheric vertical velocity, *Clim. Dyn.*, 27, 261-279, <https://doi.org/10.1007/s00382-006-0138-4>,
760 2006.

761 Yuan, T.: Increase of cloud droplet size with aerosol optical depth: An observation and modeling study, *JGR: Atmos.*,
762 113, D4, <https://doi.org/10.1029/2007JD008632>, 2008.

763 *Yang, Y., Liu, X., Qu, Y., An, J., Jiang, R., Zhang, Y., & Ma, Q. : Characteristics and formation mechanism of*
764 *continuous hazes in China: a case study during the autumn of 2014 in the North China Plain. ACP*, 15,
765 8165-8178, <https://doi.org/10.5194/acp-15-8165-2015>, 2015.

766 Zeb, B., Alam, K., Sorooshian, A., Chishtie, F., Ahmad, I., Bibi, H.: Temporal characteristics of aerosol optical
767 properties over the glacier region of northern Pakistan, *Jour. Atmos. Sol-Terr. Phy.*, 186, 35-
768 46, <https://doi.org/10.1016/j.jastp.2019.02.004>, 2019.

769 Zhao, C., Tie, X., & Lin, Y.: A possible positive feedback of reduction of precipitation and increase in aerosols
770 over eastern central China, *Geo. Res. Let.*, 33, 11, <https://doi.org/10.1029/2006GL025959>, 2006.

771 Zhou, S., Yang, J., Wang, W., Zhao, C., Gong, D., Shi, P.: An observational study of the effects of aerosols on
772 diurnal variation of heavy rainfall and associated clouds over Beijing–Tianjin–Hebei, *Atmos. Chem.*
773 *Phy.*, 20, 5211-5229, <https://doi.org/10.5194/acp-20-5211-2020>, 2020.

774